MALARIA DETECTION WITH CYCLIC CATCH-AND-RELEASE SIGNAL AMPLIFICATION

By

Michael Z. Jacobs

Thesis

Submitted to the Faculty of the

Graduate School of Vanderbilt University

in partial fulfillment of the requirements

for the degree of

MASTER OF SCIENCE

in

Biomedical Engineering

August 11, 2017

Nashville, Tennessee

Approved:

Professor Frederick R. Haselton

Professor David W. Wright

To my grandmother Elaine Sanderson, a continuous source of inspiration

and

To my parents Robin and Jonathan Jacobs,
who have always supported me in my endeavors

ACKNOWLEDGMENTS

I am truly grateful for the support from all of my family and friends that I needed to complete this work. For my family, Robin, Jonathan, Ari, Maia, and Gabe Jacobs: there are no words to describe how thankful I am for the continuous love and support from each and every one of you. To Benjy Keren, Andrew Werner, and Aaron Deutsch: thank you for your constant friendship. To Sean Bedingfield, Jon Heiselman, and Ma Luo: thanks for all of the talks, the walks, the video game playing, the coffee drinking, and the food eating. And of course, thank you Michelle for your love and support which has been a rock for me each day.

This work would not have been possible without the guidance of my advisor Rick Haselton. Thank you for always making yourself available when I was stuck and needed direction. Thank you to all of my lab members for your support. Thank you Ray Mernaugh for your support and endless knowledge. Thank you David Wright for reviewing my work. Finally, I am greatly appreciative of Tina Shaw and Amanda King, who have always promptly helped me for any number of tasks.

TABLE OF CONTENTS

LIST OF TABLES

LIST OF FIGURES

CHAPTER I

INTRODUCTION

Malaria

Malaria is a significant cause of morbidity and mortality in the tropical world, accounting for more than 500,000 deaths annually while more than 2.4 billion people are at risk of infection.[1] Most deaths occur in children under 5 years old in sub-Saharan Africa. It is endemic in 109 countries and is present in all continents except for Antarctica and Australia. It is characterized by high fevers and a flu-like illness. Malaria protozoan parasites belong to the genus *Plasmodium* and five out of 100 species in this genus are known to infect humans. In *Plasmodium falciparum, P. vivax, P. malariae, and P. ovale* the parasites are spread to people by infected female mosquitos. In *P. knowlesi* malaria is spread from monkeys to people, occurring mainly in South-East Asia.[2] *P. falciparum* is responsible for 99% of all malaria deaths, but is primarily found in Africa. *P. vivax* accounts for the second largest mortality and is primarily found outside of Africa.[2]

Elimination of malaria is a worldwide effort that began in the early 1900s and continues to this day. Malaria has been eliminated in western nations but still plagues developing countries. In the 1940s, elimination in the United States was achieved by removing mosquito breeding sites, introducing water management, and mass spraying of insecticides. After this success, a global eradication program began in 1955. However, it mainly consisted of indoor residual spraying interventions with DDT and massive, nonspecific distribution of antimalarial drugs. Although some regions experienced

intermittent transmission reductions, over time transmittance resurged in the 1960s with most mosquitos developing widespread DDT and drug resistance.[3]

Malaria control intensified in 1998 when the World Health Organization (WHO) launched the Roll Back Malaria Initiative. As a result of this initiative, malaria has been eliminated in 17 endemic countries, incidence of malaria has decreased by 41% globally since between 2000-2015, and mortality rates have declined by 62% globally between 2000 and 2015.[2] To achieve worldwide eradication, sustained elimination in all regions over an extended time period is required. In low-prevalence areas, there is an increased contribution to transmission from submicroscopic, often asymptomatic infections.[4] In some regions, submicroscopic carriers can account for up to 80% of all malaria infections.[5] These are undetectable with light microscopy and rapid diagnostic tests, the current tools to diagnose malaria in resource-limited settings. Although other technologies exist that are sensitive enough to detect submicroscopic infections, these are too complex or too expensive for point-of-care applications in resource-limited settings. Affordable, easy-to-use, and highly sensitive diagnostic tests suitable for resource-limited settings are needed if malaria eradication is to be achieved.

Malaria Life Cycle

During a blood meal, mosquitos transmit an infective sporozoite which travels through the blood and enters hepatocytes, where it begins to reproduce asexually. In *P. vivax*, the sporozoites may remain in a dormant, hypnozoite state for weeks or months. Hypnozoites are responsible for a waves of relapses typically characterized in *P. vivax*. In both *P. vivax and P. falciparum*, sporozoites will first develop into trophozoites and then into schizonts, a

process which lasts one to two weeks. Each schizont forms tens of merozoites which are released from the hepatocytes, enter the bloodstream and then invade red blood cells, initiating another asexual multiplication cycle.[6] Within red blood cells, metabolism of the parasite is dependent on the digestion of hemoglobin. Heme is produced as a result of this digestion, which is toxic to the parasites. They convert heme into hemozoin, an insoluble, crystalline pigment. A fraction of merozoites mature into gametocytes, which freely circulate in the bloodstream and are taken up and ingested by mosquitos. Merozoites which do not mature to gametocytes will develop sequentially to trophozoites, then schizonts, and finally to merozoites again which ruptures the infected red blood cell. The release of these merozoites also releases toxins that cause fevers that repeat every 24-48 hours with the life cycle of the merozoites. After merozoites are released, they infect additional red blood cells. During the erythrocytic reproductive phase, parasite proteins are exported to the surface of the red blood cell which enable the infected cells to avoid immune responses and adhere to host cells and endothelium. A *P. falciparum* infected red blood cell will express *P. falciparum* erythrocyte membrane protein 1 (PfEMP1) on its surface, which can bind to receptors on blood vessel endothelium.[7] Adherence to venules in the brain can cause congestion and impaired oxygen flow, leading to cerebral malaria and death. Furthermore, trophozoite and schizont stage parasites can sequester to the microvasculature of multiple organs including the heart, brain, liver, and placenta, causing multi-organ dysfunction.

Adherence of *P. falciparum* infected red blood cells to the vasculature reduces the effectiveness of some diagnostic tests.[4] Only young forms of the parasite are detected in peripheral blood samples. Sequestration is also synchronized, which leads to large parasite density fluctuations in and out of peripheral circulation. This can result in false-negative

results in microscopy and molecular tests due to a lack of detectable parasites and parasitic nucleic acids at the time of blood draw.[4]

Treatment of Malaria

Chloroquine is a chemotherapeutic agent first developed in the 1940s and was the first line of antimalarial treatment until its utility diminished in the 1990s due to drug resistance. It belongs to a class of quinoline antimalarial drugs, and the resistance of malaria to chloroquine also increased its resistance to other quinolone drugs. Their primary component is quinine, a complex aromatic compound first purified from cinchona bark to cure malaria in the early 1600s.[8] Quinoline compounds inhibit the parasites' conversion of digested hemoglobin into crystallized hemozoin, which increases free heme and has a toxic effect on the parasites.[9] Chloroquine's effect is so powerful that in the 1960s it was sold at low doses for many common ailments, and even as a food supplement. Its efficiency as an antimalarial agent has declined as an effect of its extensive overuse.

Chloroquine resistance has prompted many countries to adopt a new line of artemisinin drugs. Artemisinin's are a group of powerful drugs that are currently considered the standard for treating malaria, but its mechanism of action is currently unknown. One proteomics analysis has shown that artemisinin can covalently bind to 124 protein targets of the parasite, which disrupts its metabolic processes and causes parasite death.[10] The WHO explicitly discourages the use of artemisinin monotherapy, which can cause point mutations in the parasitic genome leading to drug resistance. Combination therapies are used instead, which combine one artemisinin and one chloroquine based drug.

Drug resistance is one of malaria's greatest threats to achieving eradication.

Artemisinin resistance has been discovered in Cambodia and Thailand, and there are no alternative medications to effectively take its place.[11] It is possible the resistance has developed to due widespread overuse of drugs. Fake drugs can be bought in endemic regions which contain lower levels of drugs, but not enough to kill the parasites.

Nucleic Acid Amplification Tests

Clinical diagnosis is the least expensive method to detect malaria, but symptoms often overlap with other tropical diseases, which impairs its specificity. Diagnostic tools are needed to prevent indiscriminate use of anti-malarials for febrile patients, which can increase

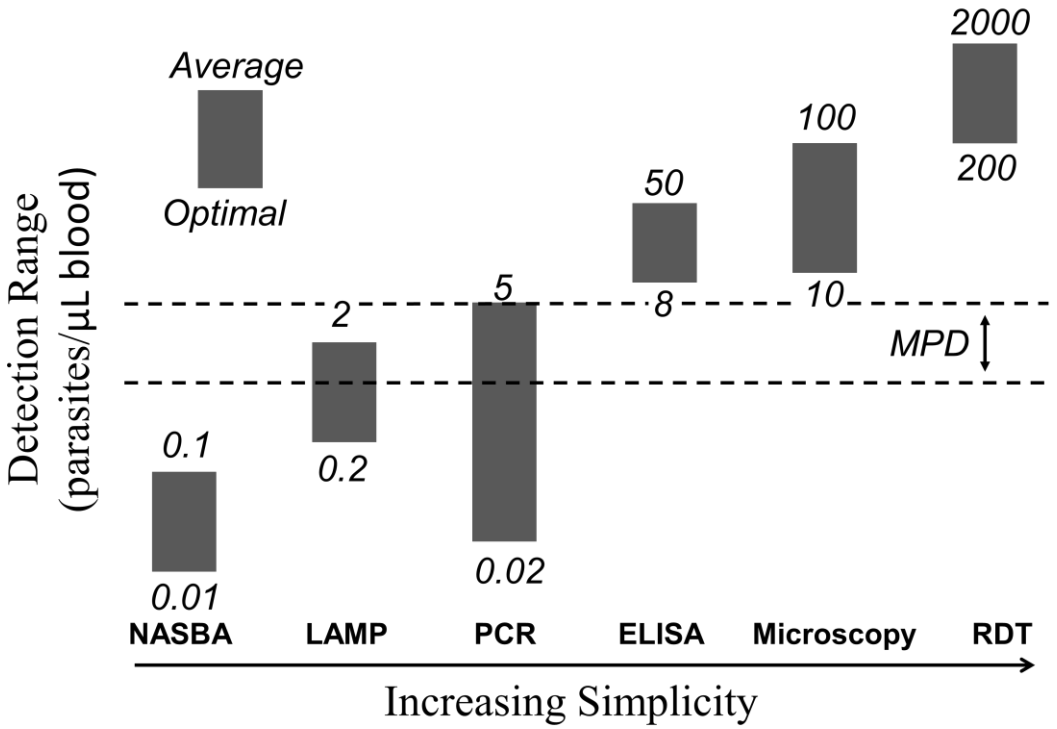

Figure 1. Sensitivity versus simplicity of malaria detection technologies. Malaria eradication is confounded by submicroscopic parasite carriers with a minimum transmissable parasite density (MPD) between ~1-5 parasites/µL blood. Although NAATs can detect MPD carriers, they are too complex for resource-limited settings. NASBA: Nucleic acid based sequence amplification. LAMP: loop mediated isothermal amplification. PCR: polymerase chain reaction. ELISA: enzyme-linked immunosorbent assay. RDT: rapid diagnostic test.[5, 12-14]

anti-malarial drug resistance. The most common malaria diagnostic tools can be divided into nucleic acid amplification tests (NAATs), optical methods, and rapid diagnostic tests (RDTs) **(Figure 1)**. NAATs are the most sensitive detection method, and can be divided into thermocyclic and isothermal amplification tests.[15-17] Light microscopy and lateral flow assays (LFAs) are the primary, field implemented optical and RDT techniques, respectively. Virtually all NAAT methods can detect a minimum of 0.05-5 parasites/μL of blood.[5] When compared to light microscopy as a reference standard, both thermocyclic and isothermal NAATs have sensitivity and specificity greater than 95%. Traditional polymerase chain reaction (PCR) is the most common thermocyclic NAAT and typically targets the 18s ribosomal RNA gene, mitochondrial DNA, and telomere repetitive element 2.[5] Despite its sensitivity, PCR is normally used only in central laboratories or peripherally to resource limited settings since it requires thermocycling and a trained technician.

Loop mediated isothermal amplification (LAMP) is a promising isothermal amplification test that can be implemented more easily in resource limited settings.[18] Isothermal amplification strategies generally require less system complexity than thermocyclers. The amplification products of LAMP are progressively larger DNA sequences that can precipitate out of solution and be visualized with fluorescence or turbidity. Although it does not require a thermocycler, it requires a constant heat source to maintain a temperature between 62-65°C. It is also prone to contamination and amplification of non-targeted DNA sequences, which has limited its application in field settings.[19] Despite the sensitivity of NAATs, they are still primarily implemented outside of malaria endemic countries.

Light Microscopy

The current gold standard of malaria diagnosis is light microscopy with Giemsa-stained blood smears.[20] It is inexpensive to perform, can differentiate malaria species, and quantify parasites. A Giemsa solution is composed of eosin and methylene blue. The eosin component stains the parasite nucleus red and methylene blue stains the cytoplasm blue. The stain is performed for two types of samples called thick and thin blood smears. In a thick blood smear, a drop of blood is stained and then viewed in a microscope at 10x or 20x objective lens to detect large parasites. A negative result can only be reported after at least 200 oil immersion fields at 1000x magnification are examined. In a thin smear, the blood is spread across a microscope slide before examination. Thick smears are useful for identifying if parasites are present, while thin smears are useful to specify the malaria species. However, it can be difficult to distinguish between certain species. For example, *P.malariae and P. knowlesi* appear similar under a microscope and other methods must be used to distinguish between the two.[21] Thick smears can detect parasitemia as low as 5 parasites/μL of blood, but tends to average between 50 and 100 for its optimal performance in the field.[20]

Giemsa stains typically require 45 minutes from blood collection to the result. Although many alternative staining methods have been developed, acridine orange (AO) is notable since it is relatively inexpensive and results are available within a few minutes.[22] AO binds to RNA and emits a red fluorescence from blue light excitation, and intraerythrocytic malaria parasites are particularly rich in RNA. However, it binds nonspecifically to RNA from all cell types, so a microscopist must be trained in distinguishing fluorescently stained parasites from other cells. Moreover, it can be especially difficult to differentiate between different parasite species. When compared against a Giemsa stain the AO method has a

sensitivity and specificity between 80-100% for high levels of parasitemia.[22] However, a decrease in sensitivity is observed for parasite concentrations below 100 parasites/μL of blood. Similarly to a Giemsa stain, 100 fields under high magnification are usually examined to reach a conclusive negative result. Since the resultant signal is fluorescent, a microscope must be equipped with a halogen lamp and an appropriate light filter.

Light microscopy is effective at detecting high concentrations of parasitemia, which has been useful for a differential diagnosis of malaria from other tropical diseases. However, it cannot sensitively detect parasitemias at concentrations seen in asymptomatic individuals, which range from 1 to 100 parasites/μl of blood.[23] Accurate diagnoses are dependent on the skill of the microscopist, and as a result there is significant variability in its sensitivity. The chance of a false negative increases with decreased experience and skill of the microscopist.[20] It is also time consuming to identify parasites at low concentration densities that require a hundred or more fields of view to be examined. Hence, many alternative diagnostic tools have been developed to assist in identifying malaria in low-resource settings.

Rapid Diagnostic Tests

RDTs, mainly LFAs, are the primary tool to screen populations for malaria. They can be easily distributed to tertiary areas where remote clinics may not have laboratories. An LFA consists of a sample pad, conjugate pad, and absorbent pad overlapped with a nitrocellulose strip, all housed in a plastic backbone **(Figure 2)**.[24] Antibodies specific to the target biomarker are immobilized on a test line on the nitrocellulose strip. Liquid sample applied to the sample pad flows by capillary force towards the opposite end of the strip. Within the conjugate pad, the target biomarker is typically labelled with a gold nanoparticle

functionalized antibody. As the sample flows through the nitrocellulose strip, the target biomarker is immobilized at the test line which forms a sandwich between the gold nanoparticle and the immobilized antibody, identical to a sandwich ELISA. Each individual immobilized antibody captures exactly one gold nanoparticle. Accumulation of gold nanoparticles at the test line causes a visible red color change due to surface plasmon resonance. Excess fluid is absorbed by the absorbent pad at the end of the LFA.[25] Most malaria LFAs are specific to a *Plasmodium* species or to a target that is conserved across all species. The most commonly targeted antigen is histidine rich protein II (HRPII), specific for *P. falciparum*. Other commonly targeted antigens include *P. falciparum*-specific lactate dehydrogenase and specific pan-*Plasmodium* targets on lactase dehydrogenase as well as aldolase enzyme.[26] HRPII readily diffuses into the plasma and can be detected at lower levels of parasitemia than panmalarial antigens. Recently, some *P. falciparum* strains have been found with the HRPII gene deleted, which has led to an increase in HRPII-specific false negative results.[27] HRPII can also persist in the bloodstream for a month after effective therapy.[28] Hence, HRPII-specific LFAs cannot be used to determine therapy effectiveness.

LFAs are important for screening populations for malaria. They require minimal operator training, can be interpreted easily, and cost less than $1 per test. As a result, they are widely adopted in resource limited settings. The WHO recommends that all individuals suspected of malaria be screened with LFAs or light microscopy.[2] At parasitemia of 1000 parasites/μL or greater, LFAs have a sensitivity and specificity of 99% and 96%. However, at parasitemia below 100 parasites/μL, the sensitivity and specificity drop to 53.9% and between 37-70%.[28] LFA performance is also affected by harsh temperature and humidity conditions. Its decreased performance at low parasitemia excludes LFAs as a viable option

to detect asymptomatic individuals. Furthermore, The WHO recommends a minimal standard of 95% sensitivity and 95% specificity for *P. falciparum* parasite densities of 100 parasites/µL of blood. Hence, LFAs do not meet the current standards of malaria detection.[28]

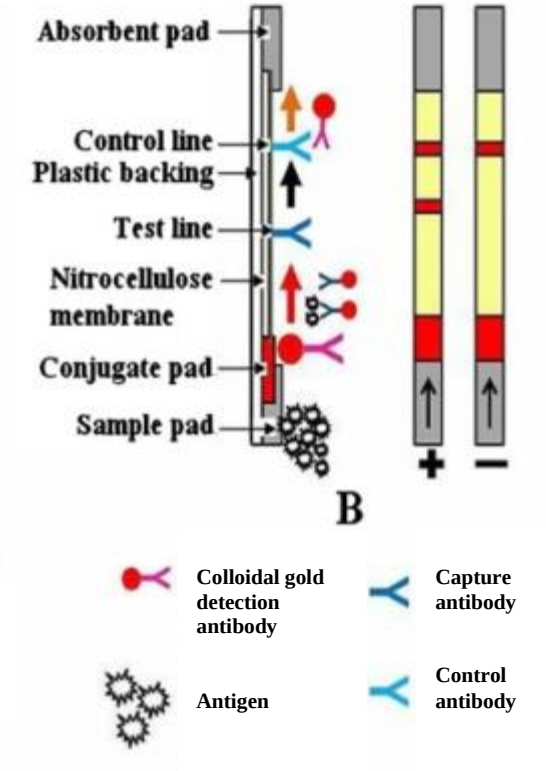

Figure 2. Lateral flow assay design.[24]

Assay Design

In an LFA, a target biomarker binds to a gold nanoparticle at a conjugate pad and flows unidirectionally on a nitrocellulose strip towards a test line via capillary flow. At the test line, the biomarker is captured by immobilized antibodies in a 1:1 ratio. If enough biomarker is captured at the test line, the immobilized gold nanoparticles will produce a color change due to surface plasmon resonance. In effect, the biomarker acts as a hook to "catch and release" gold nanoparticles from the conjugate pad to the test line. At low concentrations of biomarker, not enough gold nanoparticles are released at the test line to produce a visible signal.

We propose a new design to enable "cyclic catch-and-release." In this design, biomarker can move cyclically between a "catch" chamber and a "release" chamber. Reporter beads are captured by biomarker in the catch chamber and are eluted in the release chamber. The beads are transferred to the release chamber if and only if biomarker is present. In theory, the signal in the release chamber is amplified by *N times x*, where *N* is the number of cycles completed and *x* is the number of cycling biomarkers **(Figure 3).**

We base this design from our previous work on self-contained extraction tubes and malaria biomarker concentration strategies.[29-31] An extraction tube contains prearrayed processing solutions separated by surface tension air valves. Magnetic beads initially catch biomarker in a sample solution and are subsequently transferred into an elution chamber with an external magnet to release the biomarker. Extraction tubes are more suitable for low-resource concentration of biomarker than alternative methods such as centrifuges because they are self-contained and easy to use. Extraction tubes to date have unidirectional movement of biomarker. Bidirectional movement of biomarker has not previously been

considered.

For malaria, the target biomarker for purification is histidine rich protein II (HRPII). HRPII consists of 34% histidine, and approximately 85% of its structure is comprised of AHH and AHHAAD motifs.[32] Ni(II)nitrilotriacetic acid (NiNTA) chelation is a well-established method of coordinating polyhistidine repeats, notably for isolation and purification of his-tagged proteins. A single NiNTA molecule coordinates to two adjacent histidines with micromolar affinity.[32] NiNTA surface functionalized magnetic beads have been shown to purify and reconcentrate HRPII from blood. Concentrated HRPII can be added to HRPII specific LFAs, which improves their limit of detection 8-fold.[33-34]

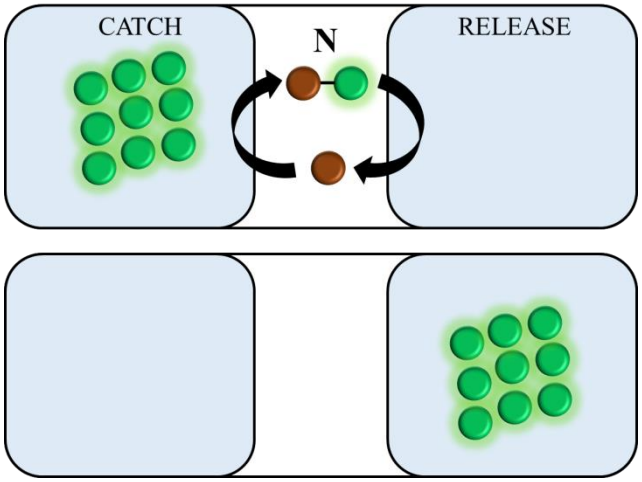

Figure 3. Cyclic catch-and-release amplification. Colorimetric beads (green) are transferred from the left to the right chamber over N cycles if and only if biomarker (brown) is present.

We propose to initially test cyclic catch-and-release amplification to detect HRPII. In our strategy, we preload tubing with a sample chamber, a catch chamber, a wash chamber, and an imidazole-rich release-detect chamber **(Figure 4)**. In the sample chamber, anti-HRPII surface functionalized magnetic beads capture HRPII. Next, the beads are transferred with an external magnet to the catch chamber containing NiNTA surface functionalized reporter

beads. The HRPII captured by magnetic beads coordinate to and catch the NiNTA reporter beads. The magnetic beads are then shuttled cyclically forward and backward between the catch and release-detect chambers. This cyclic movement transfers the reporter beads from the catch chamber to the release-detect chamber if and only if HRPII is present. The objective of this thesis is to test the performance of this strategy to detect recombinant HRPII in a self-contained prototype.

CHAPTER II

MALARIA DETECTION WITH CYCLIC CATCH-AND-RELEASE SIGNAL AMPLIFICATION

Abstract

At the onset of some infectious diseases, diagnostic biomarkers begin to circulate the bloodstream in low concentrations. Early detection of these biomarkers can improve treatment outcomes, prevent long-term complications, reduce transmissions, or screen for asymptomatic individuals. For malaria, eradication efforts have been confounded by an asymptomatic population, which cannot be diagnosed with current detection technologies such as light microscopy and lateral flow assays. We have developed a cyclic catch-and-release amplification design to detect malaria biomarker histidine rich protein II (HRPII) based on our previous work on extraction tubes and malaria catch-and-release. In this design, HRPII surface functionalized magnetic beads cyclically transfer NiNTA surface functionalized reporter beads from a "catch" chamber to an imidazole-rich "release-detect" chamber. In theory, the signal in the release-detect chamber should be amplified by N *times* x, where N is the number of cycles performed and x is the number of captured HRPII. We first created a self-contained prototype using polyhistidine functionalized magnetic beads, and demonstrated cyclic, linear amplification of NiNTA beads in the release-detect reservoir. Experimental parameters of the test were then optimized in a 96 well plate with anti-HRPII antibody functionalized magnetic beads and recombinant HRPII. The self-contained prototype was modified to incorporate the optimized parameters and antibody

functionalized beads. The final design achieved a limit of detection of 5 nM HRPII with a signal to noise ratio of 20. Overall, this study supports cyclic catch-and-release amplification as a feasible alternative for malaria detection.

Introduction

At the onset of some infectious diseases, diagnostic biomarkers begin to circulate the bloodstream in low concentrations. Early detection of these biomarkers can improve treatment outcomes, prevent long-term complications, reduce transmissions, or screen for asymptomatic individuals.[35] For malaria, asymptomatic individuals frequently have parasite concentrations below the limit of detection of light microscopy, the gold standard of malaria detection.[14, 20] Malaria eradication efforts have been confounded by submicroscopic carriers, which may contribute up to 80% of infections in an area depending on its transmission intensity.[5] The detection limit of microscopy is in the order of 100 parasites/μL of blood, and parasitemias as low as 1-5 parasties/μL of blood can contribute towards malaria transmission.[13-14]

Lateral flow assays (LFAs) are one of the most commonly implemented malaria diagnostic tests. Although they are easy-to-use and have simple visible output, they are too insensitive for eradication efforts. At parasitemias <100 parasites/μL of blood, the sensitivity and specificity of LFAs are 53.9% and between 37-70%, respectively.[28] Its decreased performance at low parasitemia excludes LFAs as a viable option to detect asymptomatic individuals. Furthermore, the WHO recommends a minimal standard of 95% sensitivity and 95% specificity for *P. falciparum* parasite densities of 100 parasites/μL of blood. Hence, LFAs do not meet the current standards of malaria detection.[28]

In an LFA, a target biomarker binds to a gold nanoparticle at a conjugate pad and flows unidirectionally on a nitrocellulose strip towards a test line via capillary flow. At the test line, the biomarker is captured by immobilized antibodies in a 1:1 ratio. If enough biomarker is captured at the test line, the immobilized gold nanoparticles will produce a color

change due to surface plasmon resonance. In effect, the biomarker acts as a hook to "catch and release" gold nanoparticles from the conjugate pad to the test line. At low concentrations of biomarker, not enough gold nanoparticles are released at the test line to produce a visible signal.

We propose a new design to enable "cyclic catch-and-release." In this design, biomarker can move cyclically between a "catch" chamber and a "release" chamber. Reporter beads are captured by biomarker in the catch chamber and are eluted in the release chamber. The beads are transferred to the release chamber if and only if biomarker is present. In theory, the signal in the release chamber is amplified by *N times x*, where *N* is the number of cycles completed and *x* is the number of cycling biomarkers **(Figure 3).**

We base this design from our previous work on self-contained extraction tubes and malaria biomarker concentration strategies.[29-31] An extraction tube contains prearrayed processing solutions separated by surface tension air valves. Magnetic beads initially catch biomarker in a sample solution and are subsequently transferred into an elution chamber with

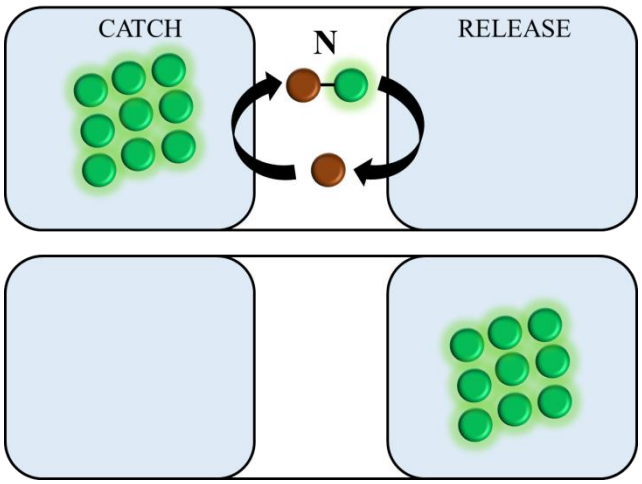

Figure 3. Cyclic catch-and-release amplification. Colorimetric beads (green) are transferred from the left to the right chamber over N cycles if and only if biomarker (brown) is present.

an external magnet to release the biomarker. Extraction tubes are more suitable for low-resource concentration of biomarker than alternative methods such as centrifuges because they are self-contained and easy to use. Extraction tubes to date have unidirectional movement of biomarker. Bidirectional movement of biomarker has not previously been considered.

For malaria, the target biomarker for purification is histidine rich protein II (HRPII). HRPII consists of 34% histidine, and approximately 85% of its structure is comprised of AHH and AHHAAD motifs.[32] Ni(II)nitrilotriacetic acid (NiNTA) chelation is a well-established method of coordinating polyhistidine repeats, notably for isolation and purification of his-tagged proteins. A single NiNTA molecule coordinates to two adjacent histidines with micromolar affinity.[32] NiNTA surface functionalized magnetic beads have been shown to purify and reconcentrate HRPII from blood. Concentrated HRPII can be added to HRPII specific LFAs, which improves their limit of detection 8-fold.[33-34]

We propose to initially test cyclic catch-and-release amplification to detect HRPII. In our strategy, we preload tubing with a sample chamber, a catch chamber, a wash chamber, and an imidazole-rich release-detect chamber **(Figure 4)**. In the sample chamber, anti-HRPII surface functionalized magnetic beads capture HRPII. Next, the beads are transferred with an external magnet to the catch chamber containing NiNTA surface functionalized reporter beads. The HRPII captured by magnetic beads coordinate to and catch the NiNTA reporter beads. The magnetic beads are then shuttled cyclically forward and backward between the catch and release-detect chambers. This cyclic movement transfers the reporter beads from the catch chamber to the release-detect chamber if and only if HRPII is present. Our objective is to test the performance of this strategy to detect recombinant HRPII in a self-contained prototype.

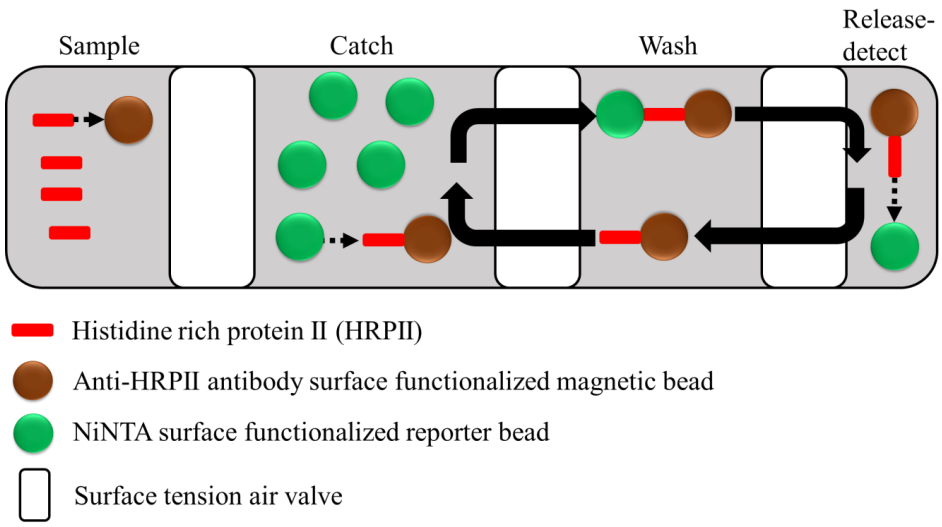

Figure 4. HRPII detection with cyclic catch-and-release amplification. Antibody surface functionalized magnetic beads initially capture HRPII in a sample solution and are shuttled to the catch chamber with an external magnet. NiNTA reporter beads coordinate to HRPII in the "catch" chamber and are eluted by a high concentration of imidazole into the "release-detect" chamber. Catch-and-release is cyclic and mediated by the bidirectional shuttling of magnetic beads between the catch and release-detect chambers. The release-detect chamber signal is proportional to the total number of cycles, *N*, and the number of HRPII on the magnetic beads.

Materials and Methods

Materials

Dynabeads MyOne Streptavidin T1 magnetic beads, mean diameter 1 µm were purchased from ThermoFisher Scientific (cat# 65601). Anti-HRP2 antibody was purchased from Abcam (cat# ab9203). Recombinant HRPII (rcHRPII) with a GST fusion tag was purchased from CTK Biosciences (cat# A3000). RcHRPII without the fusion tag was obtained from PATH. Two fluorescent NeutrAvidin-labeled polystyrene beads, 1 µm in diameter were purchased from ThermoFisher Scientific: yellow-green with excitation/emission 505/515 (cat# 8776), and red with excitation/emission 580/605 (cat #8775). Biotin N-hydroxysuccinimide ester (biotin-NHS) was purchased from Sigma-Aldrich (cat# B2643). Biotin-X-NTA was purchased from AAT Bioquest (cat# 3006). Biotin covalently attached to a six carbon spacer with terminal 8 sequential histidines (polyhistidine) was customized and purchased from GenScript. Biotin covalently attached to a six carbon spacer with a terminal glutamate was customized and purchased from GenScript.

Synthesis of polyhistidine functionalized magnetic beads

We developed polyhistidine surface functionalized magnetic beads as a simplified system of the antibody/HRPII magnetic beads. Dynabeads were washed three times with a magnetic rack and reconstituted with binding buffer (1x PBS with 0.01% Tween 20, pH 7.4), then incubated with the beads' maximum binding capacity of polyhistidine at 400 pmol polyhistidine/mg beads for 30 minutes at 4°C on a laboratory rotisserie. Next, the beads were washed three times and reconstituted with binding buffer. Free biotin was mixed with the

beads at the beads' maximum binding capacity of 1700 pmol biotin/mg of beads to block any unoccupied streptavidin sites, and the beads were incubated for 30 minutes at 4°C. The beads were washed three times with binding buffer and reconstituted with 1X PBS 0.01% BSA and 0.01% Tween 20, pH 7.4 and incubated for at least one hour at 4°C. After incubation, the beads were washed three times and reconstituted with 1x PBS 0.005% BSA and 0.01% Tween 20, pH 7.4, then stored at 4°C at a concentration of 1 mg/mL.

Synthesis of antibody functionalized magnetic beads

Biotin-NHS in dimethyl sulfoxide (DMSO) was mixed with anti-HRPII antibody at a 6:1 molar ratio and gently vortexed for 30 minutes at room temperature. The reaction was quenched with 10% volume Tris, pH 7.4. DMSO was removed from the mixture following the instructions of a 7000 MW zeba spin desalting column (ThermoFisher Scientific, cat# 89882). Dynabeads were washed three times with binding buffer. Biotinylated antibody was added to magnetic beads at the beads' maximum binding capacity of 20 μg antibody/mg beads, and the beads were incubated for one hour in binding buffer at 4°C. The magnetic beads were washed three times and reconstituted with binding buffer. Free biotin was mixed with the beads at the beads' maximum binding capacity of 1700 pmol biotin/mg of beads to block any unoccupied streptavidin sites, and the beads were incubated for 30 minutes at 4°C. The beads were washed three times with binding buffer and then reconstituted and blocked with 1x PBS 0.01% bovine serum albumin (BSA) and 0.01% Tween 20, pH 7.4 for at least one hour. The beads were washed three times with binding buffer and reconstituted with 1x PBS 0.005% BSA and 0.01% Tween 20, pH 7.4 and stored at 4°C at a concentration of 1 mg/mL.

Synthesis of NiNTA fluorescent beads

We surface functionalized 1 μm diameter fluorescent beads with NiNTA to serve as our reporter bead. We chose fluorescent rather than colorimetric beads for more accurate quantification. NeutrAvidin functionalized yellow-green polystyrene beads were washed by centrifugation (20,000 rcf, three minutes) three times and reconstituted with binding buffer. Biotin-X-NTA was added at the beads' maximum binding capacity and incubated in the dark for one hour at 4°C on a laboratory rotisserie. The maximum capacity varied by lot. For lot 1702573, the binding capacity was 2.0 nmol biotin-NTA/mg beads, and for lot 1756667 the binding capacity was 9.3 nmol biotin-NTA/mg beads. After incubation, the beads were washed two times and reconstituted with binding buffer, then mixed with free biotin at the beads' maximum binding capacity at 2.0 or 9.3 nmol biotin/mg beads for 30 minutes at 4°C. After washing the beads three times with binding buffer, they were reconstituted in 0.1 M HEPES, 0.01% Tween 20 pH 7.4. Nickel chloride was added to the suspension in a 1:1 molar ratio of nickel to available NTA sites. The solution was incubated overnight. The beads were then washed three times and reconstituted with binding buffer, then stored at 4°C at a concentration of 1 mg/mL.

Synthesis of glutamic acid fluorescent beads

To monitor nonspecific charged interactions between more positively charged, histidine rich magnetic beads and more negatively charged NiNTA reporter beads, we developed a control reporter bead. The control reporter bead was developed to have a similar negative surface charge to NiNTA beads. We expected any nonspecific bead-bead

interactions to be dominated by charged interactions. NeutrAvidin functionalized red polystyrene beads were washed by centrifugation (20,000 rcf, three minutes) three times and reconstituted with binding buffer. Biotin-glutamate was added at the beads' maximum binding capacity of 7.9 nmol biotin-glutamate/mg beads and then incubated in the dark for one hour at 4 °C on a laboratory rotisserie. The beads were washed two times and reconstituted with binding buffer, then mixed with free biotin at the beads' maximum binding capacity of 7.9 nmol biotin/mg beads for 30 minutes at 4°C. The beads were then washed two times and reconstituted with binding buffer, then stored at 4°C at a concentration of 1 mg/mL.

Test formats for catch-and-release implementation

We used three formats to investigate the properties inherent within cyclic catch-and-release amplification. The first format was in a self-contained prototype device, described below. We tested the cyclic catch-and-release amplification using polyhistidine functionalized magnetic without optimizing the experimental conditions solely for proof-of-concept. In the second format, we performed multiplexed studies in a 96 well plate for different experimental conditions to optimize our self-contained prototype for a limit of detection study. In our final test format, we used the optimized, self-contained prototype with antibody functionalized magnetic beads and determined a limit of detection.

Description of the cyclic catch-and-release device prototype

A self-contained prototype device was developed based a previous design from our laboratory **(Figure 5)**.[36-37] FEP tubing (1.6 mm inner diameter, 3.2 mm outer diameter,

purchased from Saint-Gobain, cat# TSFE14-0125-031-50) was housed between two grooved, rotating gears, one of which was press-fit to a stepper motor (Applied Motion Products, cat# HT23-597). The linear tubing contained prearrayed sample, catch, wash, and release-detect chambers separated by surface tension air valves. The motor was controlled through a ST5-Q stepper motor driver (Applied Motion Products) with commands using the Q programmer software. A program was created in Q so that the tube moved up and down in a repeated sequence. Two ¾" x ¾" x ¼" rectangular, neodymium magnets (K&J Magnetics, cat# BCC4) were fixed on a 3D printed magnet mount and placed N-S on opposite sides of the FEP tubing. This magnet design was chosen from our previous work to evenly distribute beads throughout the chambers during mixing.[38] Moving the tubing up and down between the magnets transferred the magnetic beads from one chamber to another through the air valves while leaving the liquid in the chambers fixed in place. Mixing was performed in each chamber by rapidly accelerating the tubing up and down, causing the magnetic beads to escape the magnetic field and disperse throughout the chambers. Reporter bead fluorescence in the FEP tubing was measured with a Qiagen ESElog USB fluorescence detector with dual excitation and emission filters (Qiagen, cat#9002069). Yellow-green fluorescent beads were measured with a 470 excitation and 520 emission filter. Red fluorescent beads were measured with a 565 excitation and 625 emission filter. Fluorescence measurements were obtained sequentially in order of yellow-green first and red second.

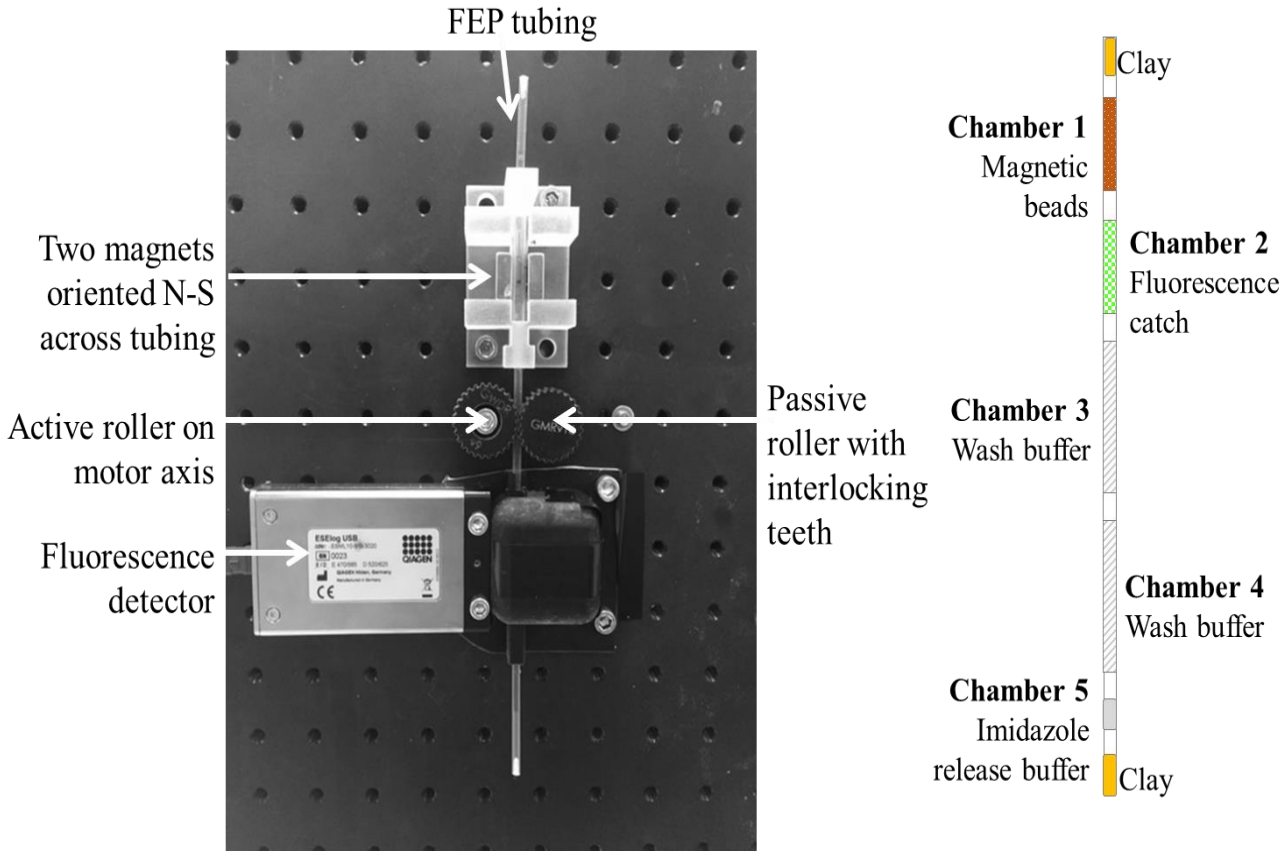

Figure 5. Left: Cyclic catch-and-release self-contained prototype. Tubing is inserted from the bottom of the 3D printed components and moved up until the magnetic beads are centered between the two magnets. Signal amplification is performed by shifting the tube up and down which shuttles the magnetic beads between a catch and release-detect chamber. **Right:** Prototype design for a cyclic catch-and-release amplification tube. Sample containing magnetic beads, catch, wash, and imidazole release buffers are separated by air valves and held in place by capping each tube end with soft clay.

At the beginning of cyclic catch-and-release, the magnetic beads were located in the sample chamber. The beads were collected by moving the tube down at a motor speed of 0.05 in/s (0.02 rps) so that the sample chamber was positioned in-between the two magnets. Then the tube was driven up at 0.05 in/s which moved the beads through an air valve and into the catch chamber. The beads were mixed by accelerating the tubing up and down rapidly with a final speed of 3.6 in/s (10 rps), which caused to beads to escape from the magnetic field. After one minute of incubation, the beads were collected, and the tube was moved up to transfer the beads into a wash chamber. In each wash step the beads were mixed by accelerating the tubing up and down. The beads were transferred through each surface tension valve by moving the tubing up at 0.05 in/s. After the final wash, the tube was moved up at 0.05 in/s until the beads were shifted to the end of the release-detect chamber. Then the tube was moved down to transfer magnetic beads back up through the wash steps until they were in the capture chamber for the next cycle. Cycles were repeated by continuously shuttling the magnetic beads back and forth between the catch and release-detect chambers in the sequence described above. Fluorescence of the release-detect chamber was measured while the magnetic beads were mixing in the catch chamber.

Proof-of-concept of cyclic catch-and-release amplification in a simplified system

In our first testing format, we performed proof-of-concept for cyclic catch-and-release amplification using a simplified system in the self-contained prototype. Biotinylated, polyhistidine compounds were surface functionalized on streptavidin coated magnetic beads in place of antibodies. This was performed to exclude complex antibody/antigen binding effects during proof-of-concept analysis. 150 µg of polyhistidine functionalized magnetic

beads were concentrated into 50 µL of 1x PBS w/ 0.1% Tween 20, pH 7.4 to create a sample chamber. A catch chamber was created by adding 10 µg of NiNTA and 10 µg of glutamate reporter beads to 50 µL of binding buffer. The FEP tubing was preloaded with the 50 µL sample chamber, the 50 µL catch chamber, two 100 µL washes, and a 20 µL imidazole release-detect chamber, each separated by 12 mm air valves. The wash chamber consisted of 1x PBS with 0.1% Tween 20, pH 7.4. The elution chamber consisted of 1x PBS with 500 mM imidazole, 300 mM NaCl, and 0.025% Tween 20, pH 8. 10 cycles of catch-and-release for three tubes were performed. Release-detect chamber fluorescence for the NiNTA and glutamate beads were quantified for each cycle.

Catch-and-release optimization studies in a 96 well plate

After demonstrating proof-of-concept, we optimized experimental parameters within 96 well plates to test multiple catch-and-release systems simultaneously. Each well in the assay is a chamber in the tubing design. Optimization of experimental parameters was performed using antibody functionalized magnetic beads. 100 µL of antibody functionalized magnetic beads was washed three times with binding buffer, and then 500 µL of 10 nM CTK rcHRPII in binding buffer were added to the beads. Another batch of 100 µL of magnetic beads was mixed with 500 µL of binding buffer only to serve as a negative control in each optimization experiment. The beads were incubated for 30 minutes on a laboratory rotisserie. After incubation, the beads were washed three times with binding buffer and reconstituted with 500 µL of binding buffer.

Optimization of reporter capture time was performed for a single cycle of catch-and-release in 96 well, black, round-bottom plates (Costar #3792). The assay was initiated by

adding 1.25 µg of rcHRPII surface captured magnetic beads and 20 µg of yellow-green NiNTA fluorescent beads to 55 µL of binding buffer (containing 150 mM NaCl) to the first three wells in row 1 of the plate. The same number of negative control beads, NiNTA beads, and binding buffer were added to the next three wells in row 1. The final volume of the wells was 100 µL. The beads were mixed in solution using a VWR standard analog shaker (VWR International, cat# 89032-092) for 2.5 minutes at 500 rpm to suspend the beads in solution. The beads were then mixed for an additional 2.5, 5, or 10 minutes at 260 rpm. To prevent spillage of beads into adjacent wells, the plate was fixed on the shaker using wooden mounts. After mixing, magnetic beads were then pulled to the side of each well with a magnetic bead separation block. The supernatant was withdrawn and dispensed into row 2. A wash consisting of 100 µL PBS 0.1% Tween 20, pH 7.4 (wash buffer) was added to the magnetic beads in column 1 and mixing was performed for 2.5 minutes at 500 rpm. Subsequently, the first wash was removed, dispensed into row 3, and a second wash was added to row 1. Mixing was performed for 2.5 minutes. After the second wash was removed and added to row 4, elution buffer consisting of 100 µL 500 mM imidazole, 300 mM NaCl, and 0.025% Tween 20 at pH 8 was added to the magnetic beads. The beads were mixed for 2.5 minutes at 500 rpm, and then for an additional 2.5 minutes at 260 rpm. The supernatant was removed and added to column 5, and then a third wash step was performed. Triplicates for 0 and 10 nM HRPII were performed in each plate and three plates were measured for each capture time. Fluorescence was measured in a BioTek Synergy HT plate reader with a 485/20 excitation and 530/25 emission filter immediately before mixing the third wash.

The number of initial NiNTA beads was optimized by adding 5, 10, 20, or 40 µg of NiNTA beads to 1.25 µg of 0 or 10 nM HRPII-captured magnetic beads in row 1 of the plate.

Binding buffer was added so that the final volume of the wells was 100 µL with a salt concentration of 150 mM NaCl. The beads were mixed for 2.5 minutes at 500 rpm and then for 2.5 minutes at 260 rpm. All other steps were performed identically to the time optimization study. Triplicates were performed for each group within each plate.

To optimize the reporter bead salt concentration, three binding buffers were created with 1x PBS, 0.01% Tween 20 at pH 7.4 with a salt concentration of 150, 300, or 450 mM NaCl. For each salt concentration, 1.25 µg of 0 or 10 nM HRPII-captured magnetic beads and 20 µg of NiNTA beads were added to 100 µL of each of the three binding buffers. Triplicates for 0 nM and 10 nM HRPII-captured beads were performed within each plate. The magnetic and fluorescent beads were mixed for 2.5 minutes at 500 rpm, and then for 2.5 minutes at 260 rpm. All other steps were performed identically to the reporter capture time optimization study.

Effects of catch chamber pH on NiNTA and glutamate bead release

The HRPII surface captured on magnetic beads have a more positive charge density compared to the NTA on the reporter beads. Any charged, nonspecific interaction between the beads in the catch chamber will be influenced by pH. Hence, we performed multiplexed, optimization studies for catch chamber pH in a 96 well plate to determine how it influenced nonspecific binding of reporter beads to magnetic beads. Optimization was performed with polyhistidine functionalized magnetic beads. 5 µg of magnetic beads were mixed with 0.5 µg of NiNTA beads and 0.5 µg of glutamate beads in 100 µL of binding buffer at pH 5, 7, 8, or 9 in a single well, in triplicates. Magnetic and fluorescent beads were mixed for 2.5 minutes at 500 rpm and then for another 2.5 minutes at 260 rpm on the VWR shaker. The

subsequent catch-and-release steps were performed identically to the reporter capture time optimization study. Yellow-green fluorescence of the catch, wash, and elution chambers were first measured with 485/20 excitation and 530/25 emission filters. Red fluorescence was measured immediately after with a 590/20 excitation and 645/40 emission filter.

Limit of detection for HRPII in the self-contained prototype.

The limit of detection for cyclic catch-and-release detection of HRPII was determined in the self-contained prototype using the optimized parameters from above. 150 µg of anti-HRPII antibody functionalized magnetic beads were washed three times and reconstituted with binding buffer in an Eppendorf tube. The supernatant was removed and 500 µL of 0, 0.1, 0.5, 1, or 5 nM of rcHRPII (PATH) in binding buffer were added to the beads. This rcHRPII was used since it does not contain a GST tag and has a molecular weight of 35 kD, similar to native HRPII.[26] The Eppendorf tube was placed on a laboratory rotisserie and incubated for 30 minutes. The beads were washed three times and reconstituted with 50 µL of 1x PBS with 150 mM NaCl, 0.1% Tween 20, pH 8. In a separate Eppendorf tube, a catch chamber was created with 10 µL of NiNTA and 10 µL of glutamate reporter beads mixed with 30 µL of 1x PBS with 0.1% Tween 20, pH 8. A tube prototype was preloaded with the magnetic beads, catch chamber, four 50 µL wash chambers, and a 20 µL elution chamber sequentially. Adjacent chambers were separated with 12 mm air valves. Four wash chambers were utilized to reduce nonspecific carryover of reporter beads. Magnetic beads were mixed in the capture chamber for one minute. Cyclic catch-and-release amplification was performed for ten cycles using the program described previously.

Statistics

Unless otherwise indicated, all error bars represent the mean +/- the standard deviation for a sample size of n=3. All tests for significance for multiple groups were performed with ANOVA. Significance was defined to be when the p-value for a comparison was $p<0.05$ at 95% confidence. The limit of detection (LOD) was defined as:

$$LOD = \sigma_{0\ nM} + 3SD_{0\ nM}$$

Where $\sigma_{0\ nM}$ is the mean 0 nM control signal and $SD_{0\ nM}$ is the standard deviation of the 0 nM control signal. An experimental group achieved the limit of detection when its signal was greater than the LOD and significantly different than the 0 nM control. For studies using only NiNTA reporter beads, the signal to noise ratio was calculated as the ratio of the test concentration over the zero control. For studies with NiNTA and glutamate reporter beads, the signal to noise ratio was calculated as the ratio of NiNTA over the glutamate signal for each test concentration.

Results

Proof-of-concept of cyclic catch-and-release amplification in a simplified system

Cyclic amplification of NiNTA reporter beads in the release-detect chamber was approximately linear over 12 cycles **(Figure 6)**. The slope of a linear fit indicated that 32,000 NiNTA beads accumulated in the release-detect chamber each cycle. This corresponded to a capture ratio of 3 NiNTA beads for every 10,000 polyhistidine functionalized magnetic beads. The glutamate beads also accumulated in the release-detect chamber linearly at a rate of 600 glutamic beads/cycle, corresponding to a capture ratio of 3 glutamate beads for every 500,000 magnetic beads. A total of 386,000 ± 91,300 NiNTA beads and 7,340 ± 2570 glutamate beads accumulated in the release-detect chamber by the 12th cycle. The difference was significant with $p<0.05$ with 95% confidence using an unpaired t-test.

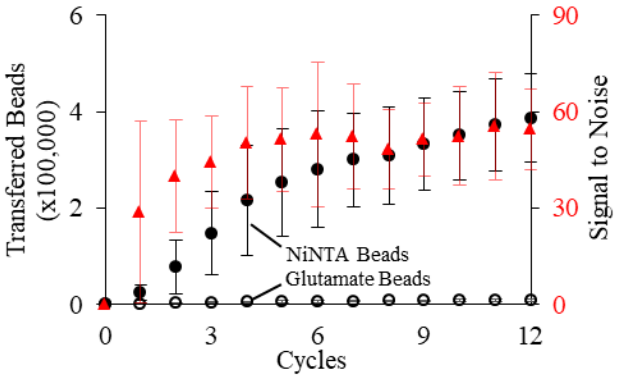

Figure 6. Cyclic catch-and-release amplification with polyhistidine functionalized magnetic beads. Release-detect chamber fluorescence is plotted for each cycle. Specific reporter beads (NiNTA, black) are compared against nonspecific reporter beads (Glu, white). Signal to noise for each cycle is indicated in red triangles.

Catch-and-release optimization studies in a 96 well plate

Increasing the reporter bead capture time had no significant effect on signal to noise **(Figure 7A)**. For 2.5, 5, and 10 minutes of capture time, the signal to noise ratio of a single cycle of catch-and-release were 19 ± 4.6, 25 ± 4.6, and 23 ± 6.0 respectively. At 5 and 10 minutes, both specific and nonspecific release of NiNTA beads was observed to increase in the release-detect chamber when compared to 2.5 minutes. 2.5 minutes was the minimum possible time to automatically maintain suspension of the magnetic and reporter beads during capture in a 96 well plate. As a result, <2.5 min was chosen as our capture time for an optimized prototype design.

Increasing the number of reporter beads in the initial capture chamber increased signal to noise only at the largest volume of beads tested **(Figure 7B).** There was no significant difference between 5, 10, and 20 µg of initial NiNTA reporter beads for a single cycle of catch-and-release, which had signal to noise ratios of 8.2 ± 2.1, 11 ± 3, and 12 ± 1.2 respectively. An initial bead mass of 40 µg substantially (but not significantly) increased the signal to noise ratio to 21.5. However, the cost of 40 µg of NiNTA reporter beads is $3.60 and the cost of 10µL is $0.80. Hence, 10 µL of reporter beads was chosen for the optimized prototype to minimize cost. 5 µL was not chosen due to the limited sensitivity of the Qiagen fluorimeter in the automated device.

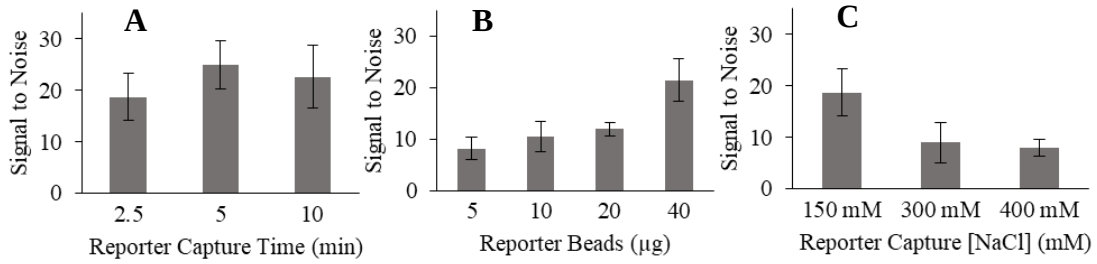

Figure 7. Optimization of reporter capture time, number of reporter beads, and reporter capture salt concentration for catch-and-release. **A.** Reporter capture time. **B.** Number of reporter beads. Signal to noise is plotted against the initial number of NiNTA beads in the catch chamber. N=2 **C.** Reporter capture salt concentration. The signal to noise is plotted against different NaCl concentrations in the catch chamber.

Signal to noise was inversely proportional to reporter capture salt concentration **(Figure 7C)**. The signal to noise ratios of 150, 300, and 400 mM NaCl in the catch chamber was 19 ± 4.6, 8.9 ± 4.6, and 7.9 ± 1.7 respectively. Increasing the salt concentration reduced the specific reporter bead signal in the release-detect chamber. Nonspecific release was reduced at lower rate than the specific signal for increased salt concentrations. 1x PBS was chosen for the optimized catch chamber buffer since 1x PBS contains 150 mM NaCl.

Effects of catch chamber pH on NiNTA and glutamate bead release

The least nonspecific carryover of glutamate reporter beads was at catch chamber pH 8 **(Figure 8)**. At low pH of 5 and 7 the nonspecific signal was 21% and 31% of that total signal, and at pH 8 and 9 the nonspecific signal was 8% and 12% of the total signal, respectively. The total number of eluted reporter beads decreased from 128,000 at pH 7 to 37,000 and 48,000 and pH 8 and 9. Hence, increasing pH of the catch chamber reduced the total signal generated in the release-detect chamber in a single cycle of catch-and-release, but it also increased the signal to noise. pH 8 had the greatest signal to noise ratio equal to 8.7. A significant difference was achieved when comparing the signal to noise ratios of pH 8 and 9 to pH 5 and 7. There was no significant difference when comparing pH 5 to pH 7 and pH 8 to pH 9.

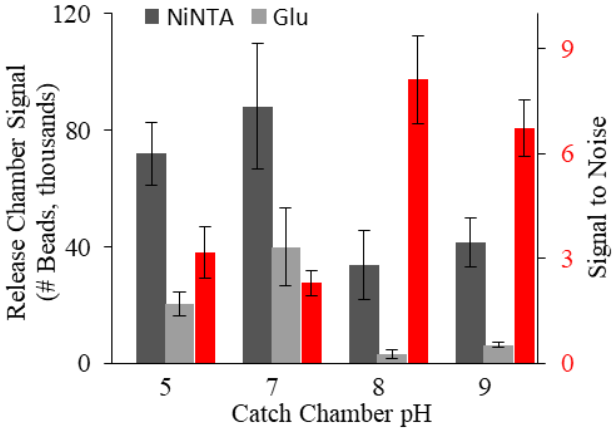

Figure 8. Effects of pH on nonspecific carryover of reporter beads. Release-detect chamber signals of specific NiNTA reporter (dark grey) and nonspecific glutamic acid (light grey) reporter beads are plotted against the pH of the reporter catch chamber. Signal to noise is represented by the red bars.

Limit of detection for HRPII in an optimized, automated prototype

The self-contained prototype was modified to incorporate the optimized parameters from the 96 well plate experiments. We initialized our experiments with 5 nM HRPII, slightly less than 10 nM HRPII from the plate optimization studies. In 10 cycles, the limit of detection was determined to be 5 nM HRPII using an ANOVA fixed-effects model, followed with pairwise t-tests. Signal to noise for 5 nM HRPII was significantly different than all other concentrations **(Figure 9)**. The number of NiNTA reporter beads in the release-detect chamber after 10 cycles for 0, 0.1, 0.5, 1, and 5 nM HRPII were 150,000 ± 56,000, 140,000 ± 47,000, 160,000 ± 61,000, 250,000 ± 25,000, and 3,000,000 ± 380,000 beads. The number of glutamate reporter beads in the release-detect chamber were not significantly different between all concentrations. There were 280, 000 ± 36,000 glutamate reporter beads in the release-detect chamber for 5 nM HRPII, significantly less than the number of NiNTA beads in 5 nM HRPII and nearly equivalent to the final number of NiNTA beads in the 0 nM HRPII control. The rates of NiNTA reporter bead amplification for 0, 0.1, 0.5, and 1.0 nM HRPII were 12,000, 12,000, 14,000, and 22,000 beads/cycle respectively, and were not significantly different. The rate of amplification for NiNTA reporter beads in 5 nM HRPII was 300,000 beads/cycle. In comparison, the rate of amplification for glutamate reporter beads with 5 nM HRPII was 23,000 beads/cycle, nearly equivalent to the rate of NiNTA bead amplification in the 0 nM control.

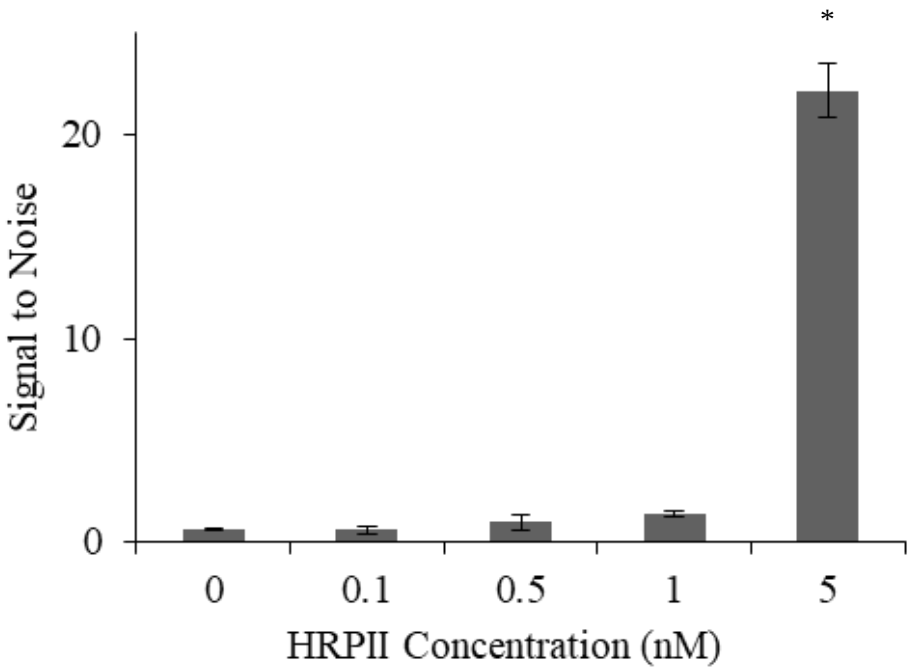

Figure 9. HRPII limit of detection study in a self-contained, prototype device. Signal to noise is plotted against increasing concentrations of HRPII.
* denotes limit of detection

Discussion

This study demonstrates the feasibility of cyclic catch-and-release amplification to detect HRPII in a self-contained prototype. Polyhistidine surface functionalized magnetic beads cyclically shuttle NiNTA reporter beads from a catch chamber to a release-detect chamber as shown by release-detect chamber signal amplification curves (Figure 6). Reporter bead concentration in the release-detect chamber increases approximately linearly after each cycle. Signal amplification for NiNTA reporter beads was significantly greater than the control glutamate reporter beads for the self-contained prototype using both polyhistidine and antibody-HRPII functionalized magnetic beads (Figures 6 and 9). With antibody functionalized magnetic beads the limit of detection was 5 nM rcHRPII. This is estimated to be equivalent to 10,000 parasites/μL of blood.[39-40] To achieve malaria eradication in resource-limited settings, more sensitive diagnostic tools are needed to detect submicroscopic malaria carriers with parasitemias between 1-5 parasites/μL of blood.[14] Although our prototype currently has a higher limit of detection, we achieved our goal of demonstrating proof-of-concept for cyclic catch-and-release amplification.

Based on our optimization studies, the following implementation was chosen for the final prototype design: 1) One minute of reporter bead capture time, 2) 10 μg of NiNTA beads and glutamate beads in the catch chamber, 3) catch chamber salt concentration of 150 mM NaCl (1x PBS), and 4) catch chamber pH 8. Optimization studies were performed with 10 nM rcHRPII, and for our final prototype our highest concentration tested was 5 nM HRPII. One minute of capture time is lower than the minimum time tested in the optimization study. In the optimization study, 2.5 minutes was the lowest time tested since it was both the minimum possible time to automate plate mixing, as well as the lowest time to sufficiently

disperse magnetic beads throughout the wells. In the self-contained prototype, we observed significant reporter bead capture in as low as one minute of capture time.

In the self-contained prototype, only one tube can be run at a time, and as a result a negative control cannot be run simultaneously to an experimental group. To monitor nonspecific carryover of reporter beads into the release-detect chamber, we developed glutamate surface functionalized reporter beads that we included in the catch chamber in the same concentration as NiNTA reporter beads. At pH 8, the charge densities of NTA and the C-terminus of glutamate are similar. Hence, the glutamate beads account for both nonspecific charged and carryover interactions between the reporter beads and more positively charged magnetic beads. In our limit of detection study, there is significantly more elution of NiNTA reporter beads than glutamate beads in the release-detect chamber at 5 nM HRPII (Figure 9), which provides evidence that the signal is not from nonspecific carryover.

At 5 nM HRPII, we achieved a signal to noise ratio equal of approximately 20, while in our simplified, polyhistidine system we achieved a signal to noise ratio of approximately 50. One reason for this phenomenon is that 300,000 polyhistidine peptides can functionalize to a single magnetic bead, while only 100,000 antibodies can functionalize to a magnetic bead. With our test conditions, our simplified system is equivalent to 400 nM HRPII, and we would expect a larger signal to noise ratio. Furthermore, our simplified system does not take into account complex antigen/antibody interactions. Our biotin-polyhistidine compounds functionalize more strongly to the streptavidin coated magnetic beads than the rcHRPII antigen binds to the antibody. Dissociation of antigen from the antibody during cyclic catch-and-release amplification could result in a reduced signal to noise ratio.

From Figure 9, it can be observed that there is a significant jump in signal to noise from 1 to 5 nM HRPII. It is plausible that under 5 nM HRPII there are not enough HRPII coordination sites available on the magnetic beads to catch reporter beads. Since the magnetic and reporter beads are extremely large compared to the HRPII that bridges them, many histidine and nickel interactions may be required within their contact radii to form a strong, dual complex. Otherwise, the reporter beads may be removed during wash steps or mixing. Each magnetic bead has approximately 100,000 antigen binding sites per bead, and hence in 5 nM HRPII there are approximately 15 HRPII available to be captured for every 100 antibodies. Thus, about 15% of the total binding sites of the magnetic beads will be available to coordinate to nickel reporter beads in the catch chamber. For sphere-sphere interactions, the contact radius *a* is equal to *1/R*, where:

$$\frac{1}{R} = \frac{1}{R_1} + \frac{1}{R_2}$$

and R1 and R2 are the radii of the two intersecting spheres.[41] With this equation, we estimated that for 5 nM HRPII approximately 1200 HRPII are surface captured on the magnetic beads within the contact radius. At 1 nM HRPII, only 239 HRPII are surface captured within the contact radius. This is limiting when compared to the number of available NiNTA sites in the contact radius of the NiNTA reporter bead, which exceeds 20,000 NiNTA. It is unknown what the minimum number of coordination bonds are needed to form a stable, dual bead complex.

Ideally, each histidine surface functionalized magnetic bead would capture at least one NiNTA reporter bead. Based on our release-detect data in the simplified system (Figure 6), we observed that approximately 3 NiNTA reporter beads were captured for every 10,000 magnetic beads and 3 glutamate reporter beads were nonspecifically captured for every

500,000 magnetic beads. Flocculation of particles have been extensively modeled.[42] In the classical Smoluchowski model, it is assumed that all collisions lead to attachment. However, an energy barrier equal to the additive short-range forces of van der Waals attraction and electrostatic repulsion must be overcome for successful attachment. The magnetic and reporter beads in our study are comprised of a negatively charged polystyrene core and theoretically results in an increased energy barrier, which would reduce the amount of NiNTA bead capture. However, histidine functionalization of the magnetic beads should more strongly lower the energy barrier for magnetic beads to bind to NiNTA beads than to glutamate beads. This matches with our results, where we observe a relatively low proportion of NiNTA beads captured per magnetic bead, but significantly more NiNTA bead capture than glutamate bead capture.

In theory, signal amplification in the release-detect chamber should remain linear over many cycles. We observed that after 5-6 cycles signal amplification decreased (Figure 6), and past 10 cycles amplification stagnated. We hypothesized that either the magnetic or the reporter beads were losing their functionality over time, which would cause less reporter beads to be captured in the catch chamber. To test this, magnetic beads and the catch chambers from experiments performed in Figure 6 were saved. When the magnetic beads were reused with new catch, wash, and release-detect chambers, they performed identically as using new magnetic beads (data not shown). However, when reused catch chambers were run with new magnetic beads, wash, and release-detect chambers, fluorescence elution was greatly diminished. Hence, it is possible that reporter release amplification decreases cyclically because of a loss in functionality of the catch chamber reporter beads. This loss in

functionality may be due to contaminants such as imidazole being introduced to the catch chamber. Further work is necessary to understand this phenomenon.

Cyclic catch-and-release amplification was automated using a computer and external software. We envision that the device can be modified to be more suitable for low-resource settings. For example, a pre-arrayed circular device can be wound up and activated similarly to an egg timer device. The device would rotate between stationary external magnets to transfer magnetic beads from one chamber to another. Colorimetric reporter beads would replace fluorescent reporter beads for field settings. After a fixed number of rotations, a diagnosis would be assessed with visual inspection of the release-detect chamber.

Conclusion

A cyclic catch-and-release amplification prototype was first developed with simplified reagents, which demonstrated cyclic amplification with a signal to noise ratio of 50. The number of magnetic beads, number of reporter beads, catch buffer salt concentration, and catch buffer pH were optimized in a 96 well plate. The prototype was modified to incorporate the optimized parameters, which achieved a limit of detection of 5 nM HRPII. With further refinement, this catch-and-release design may offer an alternative to non-amplification strategies employed in resource-limited settings.

APPENDIX A

Computer code for the self-contained prototype

The following code is used for tube movement in the simplified system and for the results described in Figure 6. The catch-and-release tube starts in an initial position where the bottom meniscus of the sample chamber is at the top of the hole of the 3D printed magnet mount. The sample chamber contains preloaded magnetic beads. In this starting position, the catch chamber should be aligned in between the two magnets. The Qiagen fluorescence program is started and run simultaneously to the motor control Q program. The sensitivity of the fluorimeter may need to be adjusted in the Qiagen program so that the fluorescence signal does not max out during cycling. Comments are included in the Q programmer code below to describe each step. Multiple catch chamber measurements are measured in each cycle as a guide to know the tube position in the fluorescence output.

Q programmer computer code

SEGMENT 1

VE	0.02	Set velocity to 0.02 rps. Tube is in starting position
FL	-13500	Move tube down 13500 steps
FL	9500	Move tube up 9500 steps – maneuver mag beads into catch chamber
EP	0	Set current position to step#0
SP	0	Set current position to step#0
QX	2	Go to segment 2

SEGMENT 2

FP	2500	Move to step# 2500
AC	10	Set acceleration to 10
VE	10	
FP	-1500	
FP	4500	Mix mag beads in catch chamber
VE	0.5	
FP	-23500	Measure catch chamber fluorescence
WT	4.00	
FP	-13000	Measure wash 1 fluorescence
WT	4.00	
FP	-23500	Measure catch chamber fluorescence
WT	2.00	
FP	2000	
WT	4.00	Measure wash 2 fluorescence
FP	-23500	
WT	2.00	
FP	15700	
WT	4.00	Measure release-detect fluorescence
FP	-23500	
WT	2.00	
FP	-1500	
QX	3	Go to segment 3

SEGMENT 3

VE	0.04	
FP	4500	
VE	0.02	
FP	9813	Move mag beads to wash 1
VE	1	
FP	19000	Mix
FP	9813	
VE	0.04	

FP	20100	
VE	0.02	Move mag beads to wash 2
FP	25982	
VE	1	Mix
FP	35000	
FP	25982	
VE	0.04	
FP	35392	
VE	0.02	
FP	43139	Move mag beads to release-detect chamber
FP	33708	Move mag beads to wash 2
VE	1	
FP	24741	Mix
FP	35708	
VE	0.04	
FP	24741	
VE	0.02	
FP	19527	Move mag beads to wash 1
VE	0.04	
FP	8538	
VE	0.02	
FP	3437	Move mag beads to catch chamber
QX	2	Go to segment 2

APPENDIX B

Limit of detection in a 96 well plate

A limit of detection study for cyclic catch-and-release amplification was conducted in a 96 well plate with the parameters characterized from the optimization study. A 10 µL 10 µM aliquot of CTK rcHRPII was diluted to 500 µL aliquots of 100 pM, 1 nM, and 10 nM HRPII in Eppendorf tubes. 25 µg of antibody functionalized magnetic beads were added to each of the 500 µL rcHRPII aliquots. In addition, 25 µg of magnetic beads were added to 500 µL of binding buffer only, which served as a negative control. The magnetic beads were incubated for 30 minutes on a laboratory rotisserie. After incubation, each group of beads were washed three times and resuspended in 500 µL of binding buffer. 100 µL from each group were added to separate wells of a 96 well plate in triplicates, and the supernatant was removed. 80 µL of binding buffer and 20 µL of NiNTA beads were added to each of the wells, in triplicates. A single cycle of catch-and-release was performed with 2.5 min of reporter capture time. Two washes were performed prior to elution and one was performed afterwards, as described in the optimization studies. Fluorescence was measured just before mixing with the third wash. After the third wash step, the second cycle was initiated by removing the third wash from row 1 and dispensing it into row 6. Then the catch chambers stored from row 2 were re-added to row 1 for another catch step. The second cycle was performed by repeating the catch, wash, and elution steps using the existing solutions in rows 2-6. Seven cycles and were performed in total **(Figure 10)**. An N of 3 was performed for each concentration. The limit of detection was determined to be 10 nM rcHRPII.

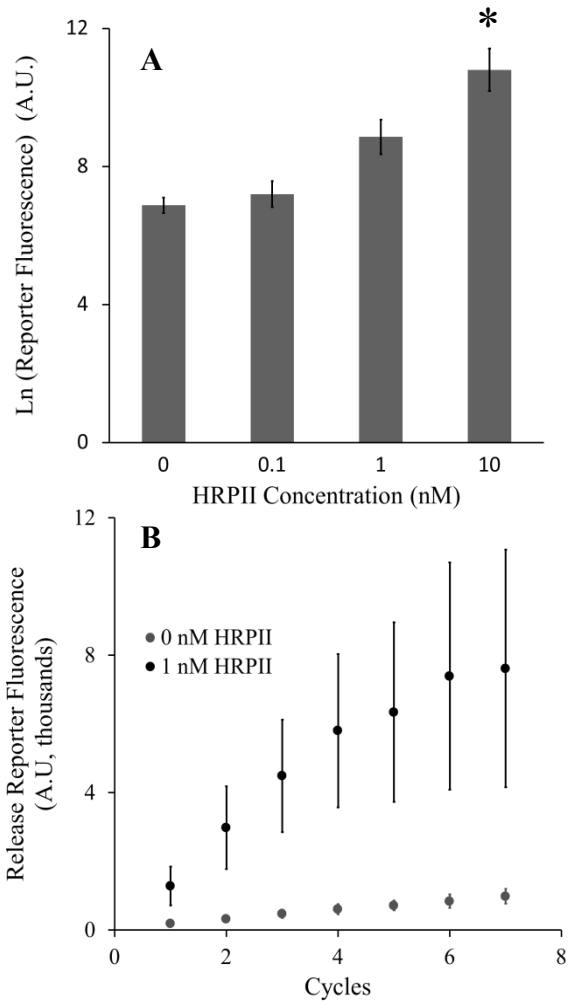

Figure 10. Cyclic catch-and-release amplification in a 96 well plate. **A.** NiNTA reporter bead fluorescence measured in the release-detect chamber after seven cycles of catch-and-release. * denotes limit of detection. **B.** Reporter bead fluorescence measured in the release-detect chamber at each cycle. NiNTA bead fluorescence is plotted against 1 nM HRPII and the negative control 0 nM HRPII.

APPENDIX C

Images of reporter bead capture

250 μg of antibody functionalized magnetic beads were washed twice with binding buffer and then added to 500 μL of 5 nM rcHRPII from PATH. Another 250 μg of magnetic beads were mixed with 500 μL of binding buffer only to serve as a negative control. The beads were incubated for 30 minutes on a laboratory rotisserie at 4°C. The supernatant was removed and the beads were washed three times with binding buffer, and then reconstituted with 500 μL of binding buffer. 100 μL of HRPII-magnetic beads and 100 μL of the negative control beads were added to separate wells in a 96 well plate. The supernatant was removed and a catch chamber consisting of 10 μg of NiNTA reporter beads in 100 μL of 1x PBS with 0.1% Tween 20, pH 8 was added to the magnetic beads. One cycle of catch-and-release was performed according to the optimization studies with a reporter catch time of 2.5 minutes, except three washes were performed before elution. Just before the elution step, 25 μL of the third wash step containing the dispersed magnetic and reporter beads were obtained from both 5 nM and 0 nM HRPII groups. 5 μL of each were added into separate wells of an eight well chamber slide (ThermoFisher Scientific, cat# 154534) containing 300 μL of binding buffer. Fluorescence images were obtained with a Nikon Eclipse microscope and a FITC filter cube (DM mirror 505, excitor 480/40, barrier 535/50, cube# 96320) and Image Pro Plus software **(Figures 11 and 12)**. In the software, an autoexposure time of 10s was applied for each picture taken.

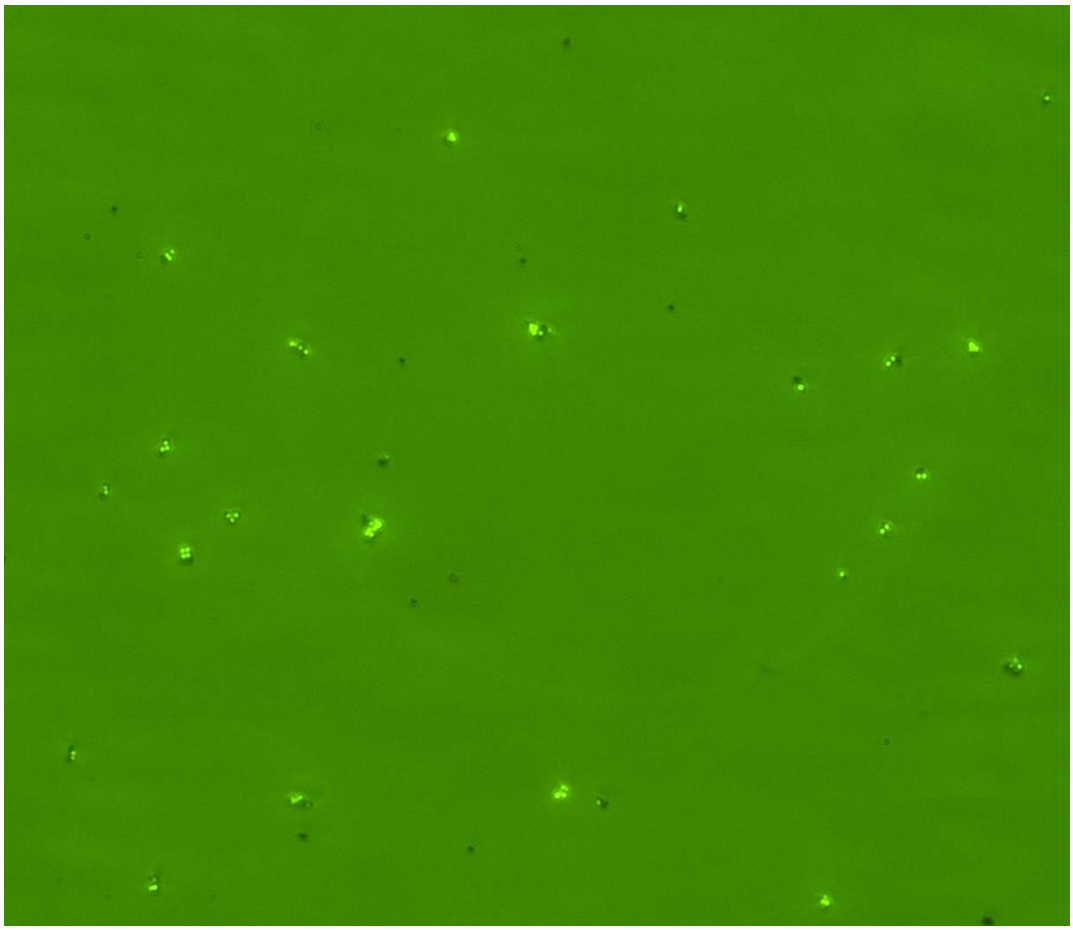

Figure 11. NiNTA reporter bead capture with 5 nM HRPII magnetic beads. Green dots: NiNTA reporter beads. Brown dots: HRPII magnetic beads. 50x.

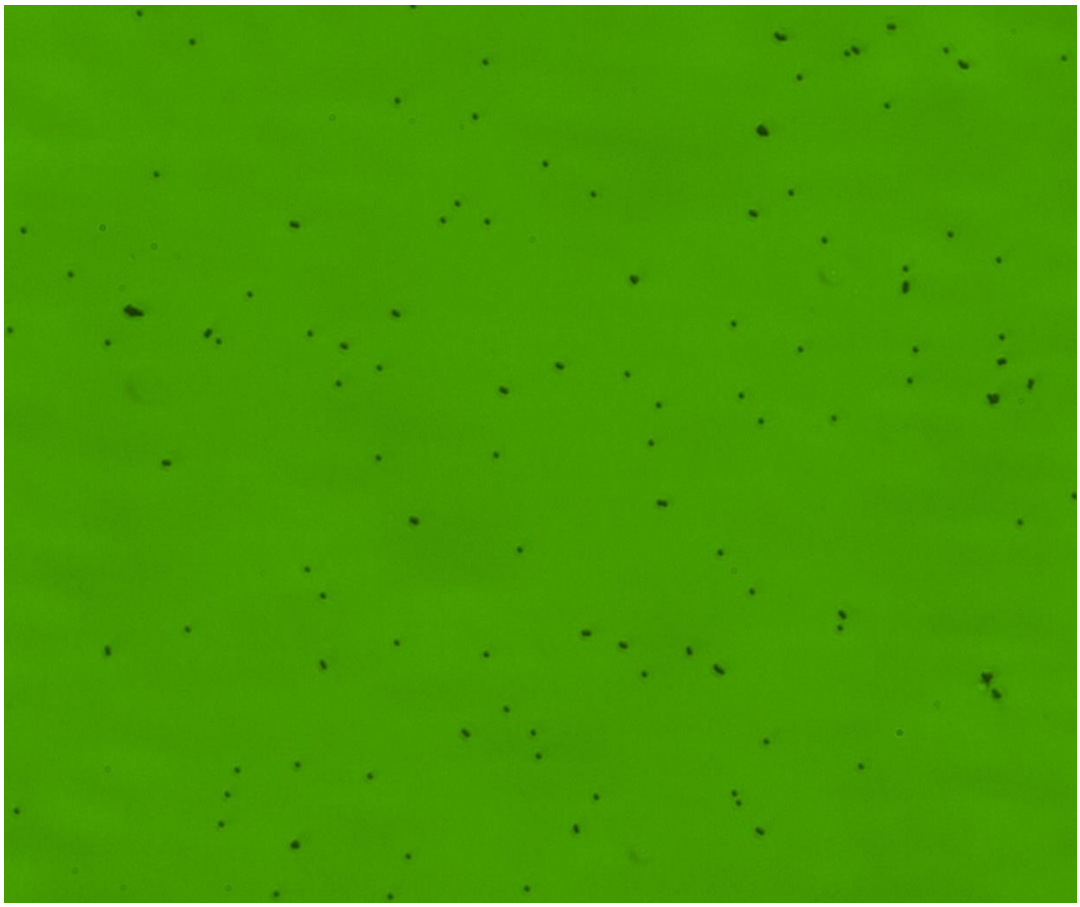

Figure 12. NiNTA reporter capture with 0 nM HRPII magnetic beads. Brown dots: HRPII magnetic beads. 50x.

APPENDIX D

Nickel detection on NiNTA reporter beads

ICP-OES

Nickel chelation of NTA functionalized reporter beads was characterized with inductively coupled plasma atomic emission spectroscopy (ICP-OES, **Figure 13**). 10 μg of NiNTA reporter beads (lot# 1756667) were centrifuged (14,000 rpm for 3 minutes) and washed three times with DI water. The supernatant was removed and 200 μL of 100 mM EDTA was added to the beads. The beads were incubated on a vortex shaker for five minutes, and then centrifuged for 3 minutes at 14,000 rpm. 100 μL of the supernatant was removed with care to not aspirate beads. The supernatant was added to 4.9 mL of 5% nitric acid. One 1 ppm and one 10 ppm solution of nickel in 5% nitric acid were created as standards. ICP-OES was then run according to the protocol below. 5% nitric acid served as a blank negative control.

No nickel was detected on the surface of the beads. This may be because the amount of nickel in the EDTA sample was close to the limit of detection for ICP-OES. For the test method described above, the final concentration of nickel in the nitric acid solution was calculated to be 2.2 μg/L, which approached the detection limit of 0.5 μg/L for nickel.

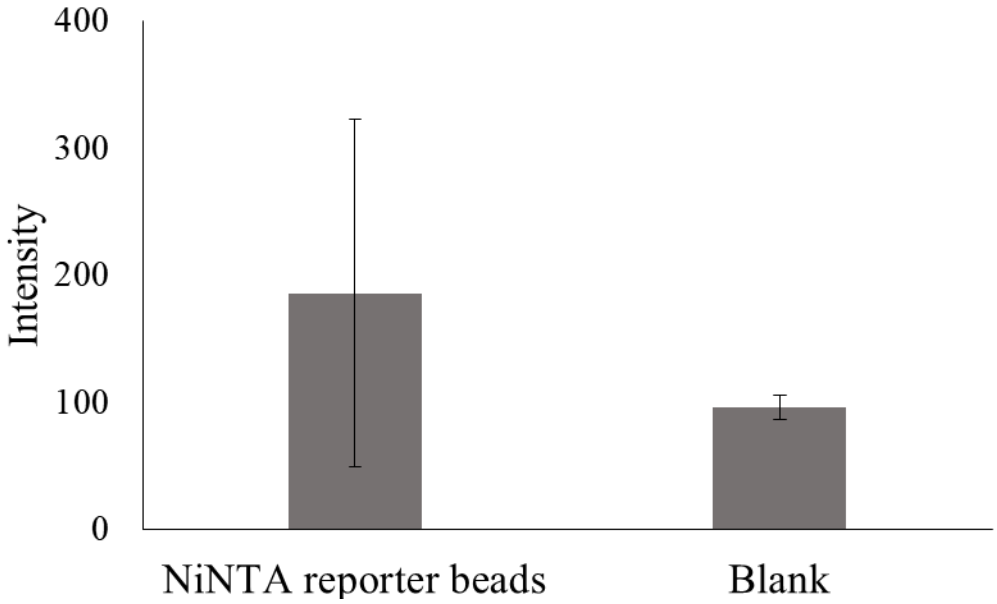

Figure 13. Nickel detection for NiNTA reporter beads with ICP-OES.

ICP-OES Instructions

- Switch on power to the various components of the system.
- Start the software and verify instrument configuration.
- Install the pump tubing so the pump is ready to start automatically once the plasma is ignited.
- Open feed of argon gas.
- Get fresh DI water beaker to rest sample feed tube.

- Ignite Plasma
- New → Method
- Default Aqueous
- Define Elements → Wavelength
    - Ni 231.604
    - Cu 327.393
    - Zn 206.200
    - Co 228.616
- Preference order indicates interference level
- Choose state
- Settings → 30 sec delay time (to allow for feed to travel through tube to torch)
- Spectrophotometer → 3 replicates
- No autosampler, No peak adjustment
- Calibration
    - Set for each element
    - Check units
- Results

    - No “start on new page” to compact results
- Manual Analysis control open
- Name results file.
- Put intake tube in blank
- Analyze blank (DI Water with 5% HNO3)
- Analyze Standards lowest to highest 10 ppb is 0.01 ppm.
- RF 1300 W Flow Rate 1.5 mL/min
- Examine → See results, look at RSD
    - Move axis to the center of peaks and green arrows to the base and narrow.
    - Update method parameters, save and update after centering each axis.
- Run one of the standards every ten samples to check for drift.

TEM-EDX

Energy dispersive spectroscopy for transmission electron microscopy (TEM-EDS) was performed to determine if nickel was chelated to the surface of the NiNTA reporter beads **(Figures 14 and 15)**. 0.1 μg of NiNTA reporter beads (lot#1756667) were washed twice and reconstituted with 100 μL of DI water. 20 μL of the beads were drop cast onto a copper mesh TEM grid and allowed to fully dry over 3-4 hours. EDX measurements were obtained by a FEI Tecnai Osiris.

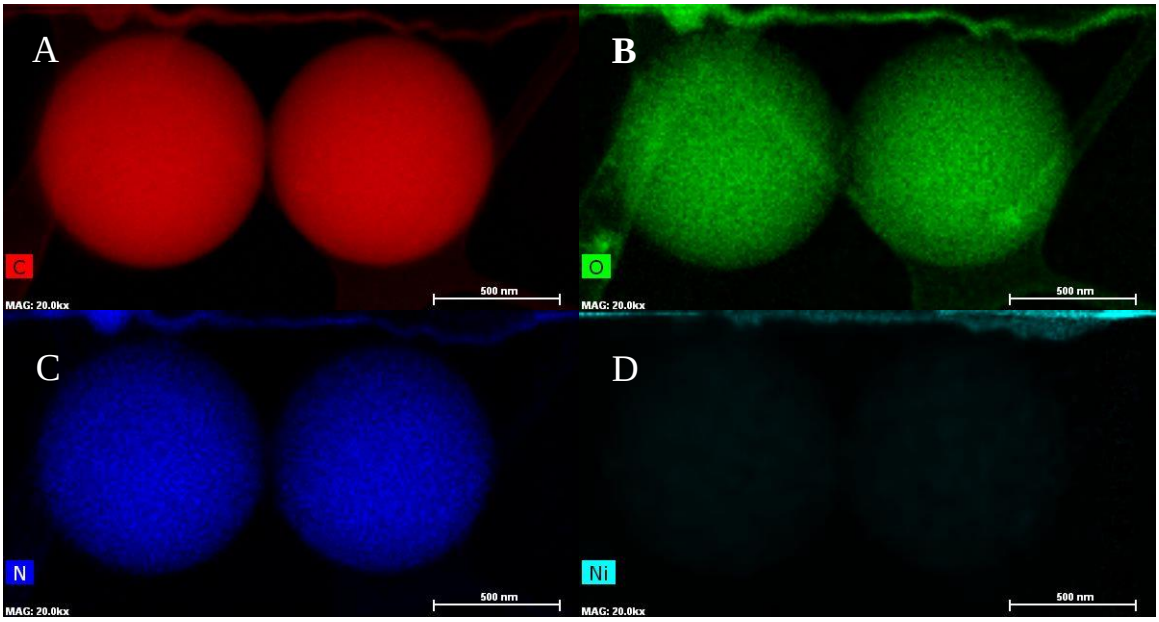

Figure 14. TEM-EDX images of two NiNTA reporter beads. **A.** Carbon. **B.** Oxygen. The copper mesh grid had an oxygen signal near the beads. **C.** Nitrogen. **D.** Nickel. Carbon, oxygen, and nitrogen were from the polystyrene core and the streptavidin surface functionalization of the beads.

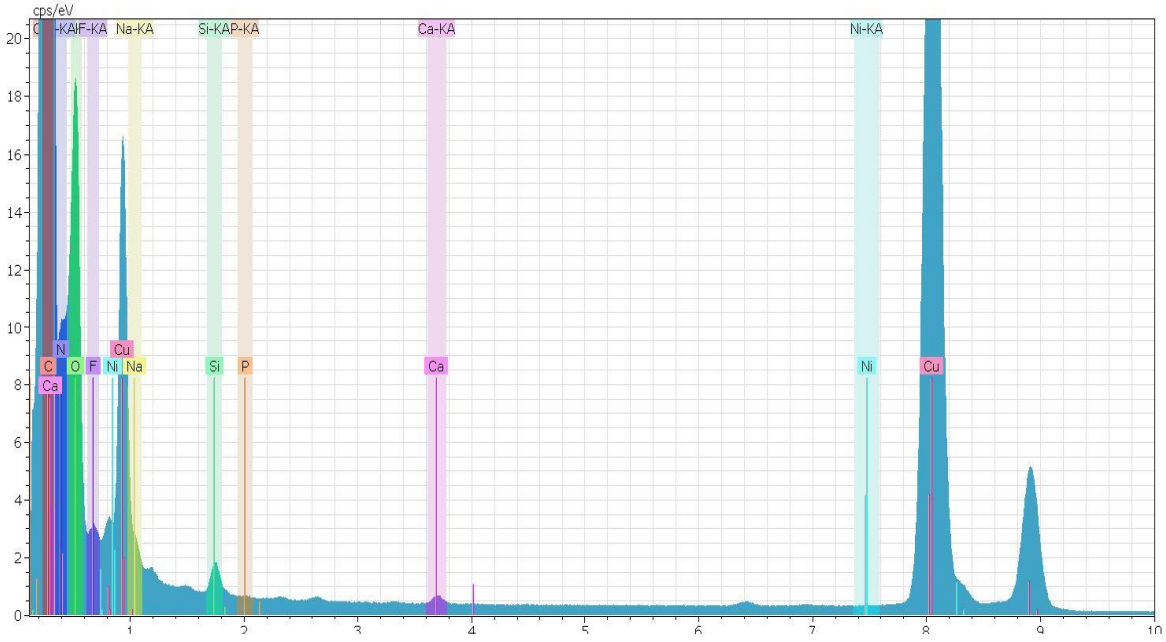

Figure 15. TEM-EDX spectra of NiNTA reporter beads. The intense copper and medium silicon peaks were from the copper mesh grid. Cadmium peaks were a result of mesh contamination. The iron peak was noise from the instrument.

APPENDIX E

Characterization of magnetic bead functionality

Polyhistidine

Biotin-polyhistidine functionalization of magnetic beads was characterized with NiNTA horseradish peroxidase (HRP, ThermoFisher Scientific, cat# 15165), which was diluted 1:500 with 1x PBS, 0.1% Tween 20, pH 7.4. 25 μg of polyhistidine functionalized beads and 25 μg of biotin functionalized magnetic beads were added to separate wells of a clear, 96 well plate. The beads were washed twice with 1x PBS with 0.1% Tween 20, pH 7.4 and then reconstituted with 100 μL of NiNTA HRP. After 10 minutes of incubation, the beads were washed twice and then reconstituted with 100 μL of ABTS/H_2O_2. Absorbance was read at 450 nm with a Synergy HT plate reader after a minimum incubation time of 10 minutes **(Figure 16)**.

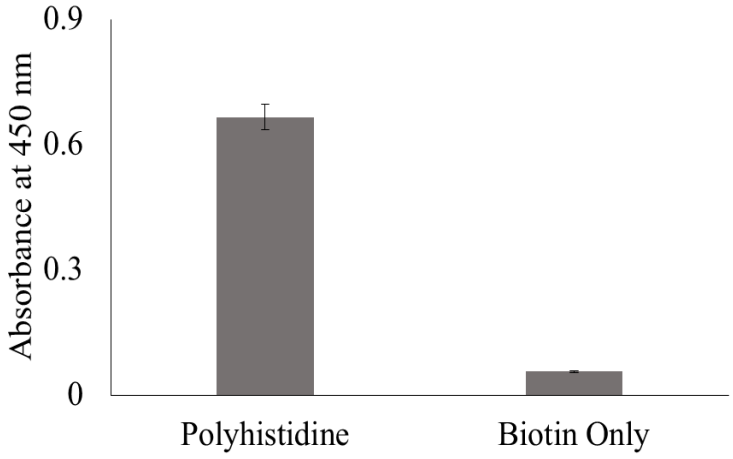

Figure 16. Absorbance after the addition of ABTS/H_2O_2 to NiNTA HRP/polyhistidine-bead complexes.

Anti-HRPII antibody

Anti-HRPII antibody functionalization of magnetic beads was characterized with goat anti-mouse IgG HRP (Sigma-Aldrich, cat# A0168). The anti-IgG HRP was diluted 1:1000 in 1x PBS and 0.1% Tween 20, pH 7.4. 25 µg of antibody functionalized beads and 25 µg of biotin functionalized beads were added to separate wells of a clear, 96 well plate. The beads were washed twice with 1x PBS with 0.1% Tween 20, pH 7.4, and then reconstituted with 100 µL of anti-IgG HRP. The beads were then incubated for a minimum of 10 minutes. Next, they were washed with 1x PBS with 0.1% Tween 20, pH 7.4, and then reconstituted with 300 µL of ABTS/H_2O_2. Color change was measured with the Synergy HT plate reader with 450 nm absorbance after 30 minutes **(Figure 17)**.

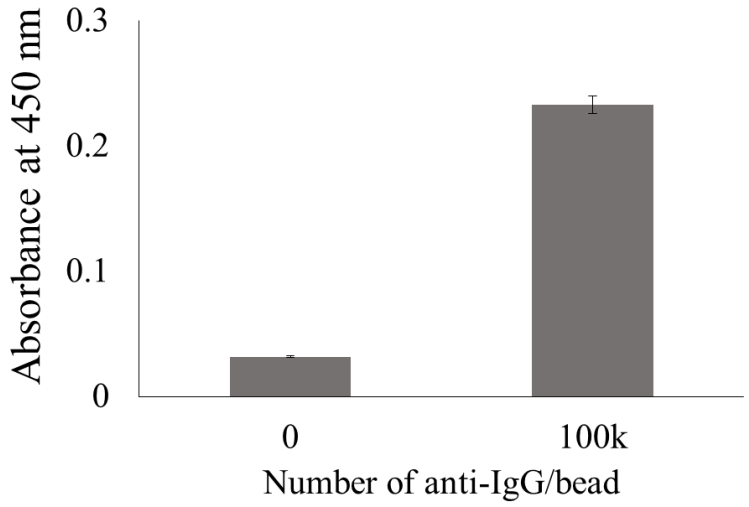

Figure 17. Absorbance after the addition of ABTS/H_2O_2 to anti-IgG HRP/anti-HRPII bead complexes.

HRPII

HRPII conjugation to antibody functionalized magnetic beads was characterized with NiNTA HRP. The NiNTA HRP was diluted 1:250 in 1xPBS with 0.1% Tween 20, pH 7.4. 100 µg of antibody functionalized magnetic beads were incubated with 0, 1, 10, or 100 nM of CTK rcHRPII in 500 µL binding buffer for 30 minutes. The beads were then washed three times with binding buffer. 25 µg of beads from each HRPII concentration were added to separate wells in a clear, 96 well plate and washed two more times with 1x PBS with 0.1% Tween 20, pH 7.4. The wash buffer was removed and the beads were then incubated with 100 µL of NiNTA HRP for 10 minutes. The beads were washed twice and then 300 µL of ABTS/H_2O_2 were added to each well. After 30 minutes of incubation, absorbance at 450 nm was measured with a Synergy HT plate reader **(Figure 18)**.

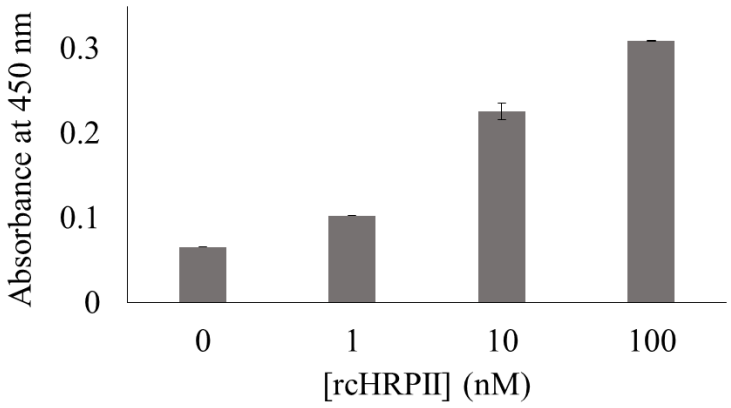

Figure 18. Absorbance after the addition of ABTS/H_2O_2 to NiNTA HRP/HRPII-bead complexes.

APPENDIX F

Zeta potential measurements of magnetic and reporter beads

Chemical groups on the surfaces of beads can vary in their charge and can influence nonspecific, charged interactions. Surface charges for magnetic and reporter beads were measured with a Malvern Nano ZS **(Table 1)**. A universal dip cell shared by VINSE was obtained for these measurements. 5 μg of polyhistidine magnetic beads, NiNTA reporter beads, or glutamate reporter beads were added to separate disposable, polystyrene cuvettes containing 1 mL of 0.1x PBS (~15 mM NaCl), pH 8. The beads were vortexed for 10 seconds prior to their addition in the cuvettes. A zeta potential SOP was created with the following settings: material: polystyrene latex; dispersant: water; general options – model – Smoluchowski; temperature: 25 °C; cell type: DTS1070 zeta dip cell; measurement: minimum runs = 10, maximum runs = 100, number of measurements = 3, and delay between measurements = 5 seconds. For each trial, the dip cell was first cleaned by sonicating the electrodes for 3-5 minutes, scrubbing the electrodes with pipe cleaner until the electrodes looked clean by visual inspection, and then air drying the electrodes. This cleaning process was repeated if necessary to clean the electrodes further. A cuvette containing beads was sonicated for 30 seconds, and the dip cell was added to the cuvette. The cuvette was then added to the zetasizer, and the protocol described above was run. After each series of three measurements the dip cell was cleaned as described above.

Beads	Zeta Potential
Polyhistidine magnetic beads	-16 ± 0.95
Glutamate reporter beads	-23 ± 1.1
NiNTA reporter beads	-39.6 ± 1.5

Table 1. Particle zeta potentials after surface functionalization.

APPENDIX G

Reporter bead saturation in the release-detect reservoir

We observed that the reporter release amplification in the release-detect reservoir began to decrease after 3-4 cycles (Figure 6). Chambers from experiments performed as described for the simplified system tests were saved. Saved polyhistidine magnetic beads were added to a self-contained prototype with new catch, wash, and release-detect chambers, and cyclic catch-and-release amplification was performed. We observed similar performance of cyclic catch-and-release compared to when new magnetic beads were used **(Figure 19)**. Therefore, magnetic beads do not lose their reporter capture functionality over time.

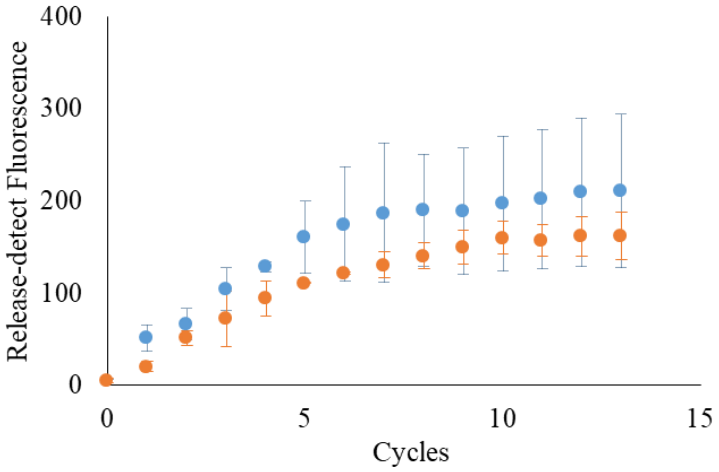

Figure 19. Effect of rerun magnetic beads on reporter release amplification. Polyhistidine magnetic beads run in a second cyclic catch-and-release experiment (orange) perform similarly to those run in only one experiment (blue).

Next, catch chambers were saved from simplified catch-and-release assays that were run for one or two hours. They were added to a self-contained prototype containing new polyhistidine magnetic beads, new washes, and a new release-detect chamber. Cyclic catch-and-release amplification was then performed for 12 cycles. We observed that catch chambers from the two hour assay resulted in decreased release per cycle than the expected values from the simplified system experiments **(Figure 20).** Catch chambers in the one hour assay performed similarly to the expected values. Hence, changes in the catch chamber over time may lead to a progressive decrease in reporter release amplification. This may be due to cycle-dependent contamination of the catch chamber, leaching of chelated nickel from the catch chamber reporter beads, or due to a subset of nonfunctional reporter beads that cannot be captured.

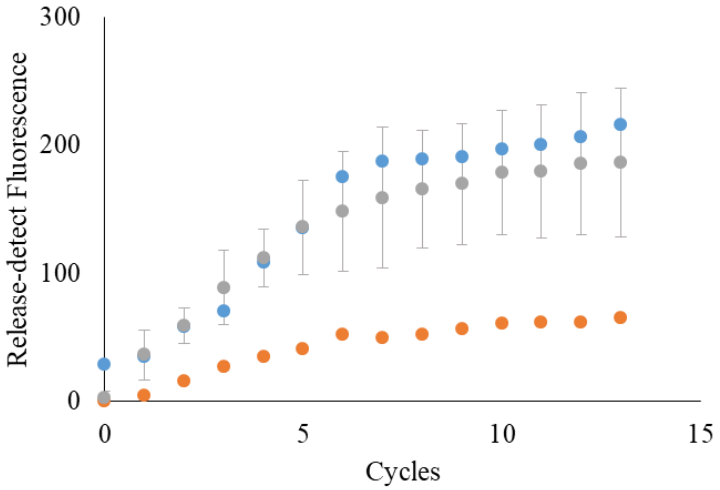

Figure 20. Effect of rerun catch chambers on reporter release amplification. Catch chambers used after two hours of cyclic catch-and-release (orange, n=1) resulted in decreased release per cycle than experiments performed in the simplified proof-of-concept study (grey, n=3). Catch chambers used after one hour (blue, n=1) performed similarly.

It is possible that after performing cyclic catch-and-release for many cycles that the concentration of catch chamber reporter beads diminishes to a level which limits reporter capture. As a result, reporter release would decrease over time. We increased the starting concentration of reporter beads 10 fold to observe if the reporter release amplification decreased over time. After 12 cycles, we observed that reporter release amplification still decreased over time, despite a sufficient concentration of reporter beads in the catch chamber each cycle **(Figure 21)**.

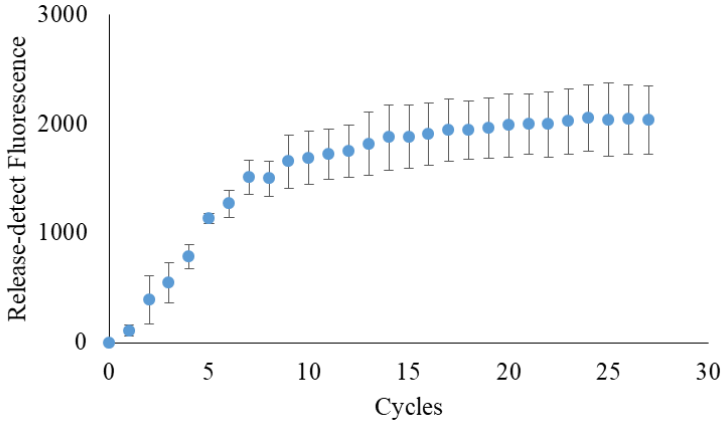

Figure 21. Effects of increased reporter bead starting concentration on reporter release amplification. Reporter release amplification decreased cyclically after the reporter bead starting concentration was increased 10 fold.

REFERENCES

(1) Bousema, T.; Drakeley, C., Epidemiology and infectivity of Plasmodium falciparum and Plasmodium vivax gametocytes in relation to malaria control and elimination. *Clinical Microbiology Reviews* **2011,** *24*, 377-410.

(2) WHO *World Malaria Report*; World Health Organization: Geneva, 2016.

(3) Nájera, J. A.; González-Silva, M.; Alonso, P. L., Some lessons for the future from the global malaria eradication programme (1955-1969). *PLoS Medicine* **2011,** *8* (1), 1-7.

(4) Tietje, K.; Hawkins, K.; Clerk, C.; Ebels, K.; McGray, S.; Crudder, C.; Okell, L.; LaBarre, P., The essential role of infection-detection technologies for malaria elimination and eradication. *Trends in Parasitology* **2014,** *30* (5), 259-266.

(5) Zimmerman, P. a.; Howes, R. E., Malaria diagnosis for malaria elimination. *Current opinion in infectious diseases* **2015,** *28* (5), 446-454.

(6) Miller, L. H.; Baruch, D. I.; Marsh, K.; Doumbo, O. K., The pathogenic basis of malaria. *Nature* **2002,** *415*, 673-679.

(7) Rowe, J. A.; Claessens, A.; Corrigan, R. A.; Arman, M., Adhesion of Plasmodium falciparum-infected erythrocytes to human cells: molecular mechanisms and therapeutic implications. *Expert Reviews in Molecular Medicine* **2009,** *11* (e16), 1-29.

(8) Schalkwyk, D. A. V.; Alphonse, C. L., History of Antimalarial Agents. *eLS* **2015**, 10.1002/9780470015902.a0003624.pub3.

(9) Combrinck, J. M.; Mabotha, T. E.; Ncokazi, K. K.; Ambele, M. A.; Taylor, D.; Smith, P. J.; Hoppe, H. C.; Egan, T. J., Insights into the role of heme in the mechanism of action of antimalarials. *ACS chemical biology* **2013,** *8* (1), 133-7.

(10) Wang, J.; Zhang, C.-J.; Chia, W. N.; Loh, C. C. Y.; Li, Z.; Lee, Y. M.; He, Y.; Yuan, L.-X.; Lim, T. K.; Liu, M.; Liew, C. X.; Lee, Y. Q.; Zhang, J.; Lu, N.; Lim, C. T.; Hua, Z.-C.; Liu, B.; Shen, H.-M.; Tan, K. S. W.; Lin, Q., Haem-activated promiscuous targeting of artemisinin in Plasmodium falciparum. *Nature Communications* **2015,** *6*, 10111.

(11) Enserink, M., Malaria's Drug Miracle in Danger. *Science* **2010,** *328* (5980), 844-846.

(12) PATH *Malaria Diagnostics Technology Landscape: Enzyme Linked Immunosorbent Assays (ELISA) for Histidine Rich Protein 2 (HRP 2)*; PATH: Seattle, WA, 2014.

(13) WHO, Policy brief on malaria diagnostics in low-transmission settings. **2014**, 1-12.

(14) Lindblade, K. A.; Steinhardt, L.; Samuels, A.; Kachur, S. P.; Slutsker, L., The silent threat: asymptomatic parasitemia and malaria transmission. *Expert Review of Anti-infective Therapy* **2013,** *11*, 623-639.

(15) Oriero, E. C.; Jacobs, J.; Van Geertruyden, J. P.; Nwakanma, D.; D'Alessandro, U., Molecular-based isothermal tests for field diagnosis of malaria and their potential contribution to malaria elimination. *The Journal of antimicrobial chemotherapy* **2015,** *70* (1), 2-13.

(16) Vasoo, S.; Pritt, B. S., Molecular diagnostics and parasitic disease. *Clinics in Laboratory Medicine* **2013,** *33*, 461-503.

(17) Roth, J. M.; Korevaar, D. A.; Leeflang, M. M.; Mens, P. F., Molecular malaria diagnostics: A systematic review and meta-analysis. *Critical reviews in clinical laboratory sciences* **2016,** *53* (2), 87-105.

(18) Han, E. T., Loop-mediated isothermal amplification test for the molecular diagnosis of malaria. *Expert review of molecular diagnostics* **2013,** *13* (2), 205-18.

(19) Morris, U.; Khamis, M.; Aydin-Schmidt, B.; Abass, A. K.; Msellem, M. I.; Nassor, M. H.; González, I. J.; Mårtensson, A.; Ali, A. S.; Björkman, A.; Cook, J., Field deployment of loop-mediated isothermal amplification for centralized mass-screening of asymptomatic malaria in Zanzibar: a pre-elimination setting. *Malaria Journal* **2015,** *14*, 205.

(20) Wongsrichanalai, C.; Barcus, M. J.; Muth, S.; Sutamihardja, A.; Wernsdorfer, W. H., A Review of Malaria Diagnostic Tools: Microscopy and Rapid Diagnostic Test (RDT). *The American Journal of Tropical Medicine and Hygiene* **2007,** *77* (6), 119-127.

(21) McCutchan, T. F.; Piper, R. C.; Makler, M. T., Use of Malaria Rapid Diagnostic Test to Identify Plasmodium knowlesi Infection. *Emerging Infectious Diseases* **2008,** *14* (11), 1750-1752.

(22) Keiser, J.; Utzinger, J.; Premji, Z.; Yamagata, Y.; Singer, B. H., Acridine Orange for malaria diagnosis: its diagnostic performance, its promotion and implementation in Tanzania, and the implications for malaria control. *Annals of tropical medicine and parasitology* **2002,** *96* (7), 643-54.

(23) Bousema, T.; Okell, L.; Felger, I.; Drakeley, C., Asymptomatic malaria infections: detectability, transmissibility and public health relevance. *Nature Reviews Microbiology* **2014,** *12*, 833-840.

(24) Ngom, B.; Guo, Y.; Wang, X.; Bi, D., Development and application of lateral flow test strip technology for detection of infectious agents and chemical contaminants: A

review. *Analytical and Bioanalytical Chemistry* **2010,** *397*, 1113-1135.

(25) Moody, A., Rapid Diagnostic Tests for Malaria Parasites. *Clinical Microbiology Reviews* **2002,** *15* (1), 66-78.

(26) Jain, P.; Chakma, B.; Patra, S.; Goswami, P., Potential Biomarkers and Their Applications for Rapid and Reliable Detection of Malaria. *BioMed research international* **2014,** *2014*, 1-20.

(27) Kumar, N.; Pande, V.; Bhatt, R. M.; Shah, N. K.; Mishra, N.; Srivastava, B.; Valecha, N.; Anvikar, A. R., Genetic deletion of HRP2 and HRP3 in Indian Plasmodium falciparum population and false negative malaria rapid diagnostic test. *Acta tropica* **2013,** *125* (1), 119-21.

(28) Murray, C. K.; Gasser, R. a.; Magill, A. J.; Miller, R. S., Update on rapid diagnostic testing for malaria. *Clinical Microbiology Reviews* **2008,** *21*, 97-110.

(29) Bordelon, H.; Adams, N. M.; Klemm, A. S.; Russ, P. K.; Williams, J. V.; Talbot, H. K.; Wright, D. W.; Haselton, F. R., Development of a low-resource RNA extraction cassette based on surface tension valves. *ACS Applied Materials and Interfaces* **2011,** *3*, 2161-2168.

(30) Adams, N. M.; Bordelon, H.; Wang, K. K. A.; Albert, L. E.; Wright, D. W.; Haselton, F. R., Comparison of three magnetic bead surface functionalities for RNA extraction and detection. *ACS Applied Materials and Interfaces* **2015,** *7*, 6062-6069.

(31) Bordelon, H.; Ricks, K. M.; Pask, M. E.; Russ, P. K.; Solinas, F.; Baglia, M. L.; Short, P. A.; Nel, A.; Blackburn, J.; Dheda, K.; Zamudio, C.; Cáceres, T.; Wright, D. W.; Haselton, F. R.; Pettit, A. C., Design and use of mouse control DNA for DNA biomarker extraction and PCR detection from urine: Application for transrenal Mycobacterium tuberculosis DNA detection. *Journal of Microbiological Methods* **2017,** *136*, 65-70.

(32) Gulka, C. P.; Swartz, J. D.; Wright, D. W., Ni(II)NTA AuNPs as a low-resource malarial diagnostic platform for the rapid colorimetric detection of Plasmodium falciparum Histidine-Rich Protein-2. *Talanta* **2015,** *135*, 94-101.

(33) Davis, K. M.; Swartz, J. D.; Haselton, F. R.; Wright, D. W., Low-resource method for extracting the malarial biomarker histidine-rich protein II to enhance diagnostic test performance. *Analytical chemistry* **2012,** *84* (14), 6136-42.

(34) Ricks, K. M.; Adams, N. M.; Scherr, T. F.; Haselton, F. R.; Wright, D. W., Direct transfer of HRPII-magnetic bead complexes to malaria rapid diagnostic tests significantly improves test sensitivity. *Malaria Journal* **2016,** *15*, 399.

(35) Banoo, S.; Bell, D.; Bossuyt, P.; Herring, A.; Mabey, D.; Poole, F.; Smith, P. G.;

Sriram, N.; Wongsrichanalai, C.; Linke, R.; O'Brien, R.; Perkins, M.; Cunningham, J.; Matsoso, P.; Nathanson, C. M.; Olliaro, P.; Peeling, R. W.; Ramsay, A., Evaluation of diagnostic tests for infectious diseases: general principles. *Nature Reviews Microbiology* **2006,** *4*, S21-S31.

(36) Russ, P. K.; Karhade, A. V.; Bitting, A. L.; Doyle, A.; Solinas, F.; Wright, D. W.; Haselton, F. R., A Prototype Biomarker Detector Combining Biomarker Extraction and Fixed Temperature PCR. *Journal of laboratory automation* **2016,** *21*, 590-8.

(37) Creecy, A.; Russ, P. K.; Solinas, F.; Wright, D. W.; Haselton, F. R., Tuberculosis Biomarker Extraction and Isothermal Amplification in an Integrated Diagnostic Device. *Plos One* **2015,** *10*, 1-14.

(38) Scherr, T. F.; Ryskoski, H. B.; Doyle, A. B.; Haselton, F. R., A two-magnet strategy for improved mixing and capture from biofluids. *Biomicrofluidics* **2016,** *10*, 024118.

(39) Gulka, C. P.; Swartz, J. D.; Trantum, J. R.; Davis, K. M.; Peak, C. M.; Denton, A. J.; Haselton, F. R.; Wright, D. W., Coffee rings as low-resource diagnostics: detection of the malaria biomarker Plasmodium falciparum histidine-rich protein-II using a surface-coupled ring of Ni(II)NTA gold-plated polystyrene particles. *ACS applied materials & interfaces* **2014,** *6* (9), 6257-63.

(40) Trantum, J. R.; Wright, D. W.; Haselton, F. R., Biomarker-mediated disruption of coffee-ring formation as a low resource diagnostic indicator. *Langmuir: the ACS journal of surfaces and colloids* **2012,** *28*, 2187-93.

(41) Hanaor, D. A. H.; Gan, Y.; Einav, I., International Journal of Solids and Structures Contact mechanics of fractal surfaces by spline assisted discretisation. *International Journal of Solids and Structures* **2015,** *59*, 121-131.

(42) Thomas, D. N.; Judd, S. J.; Fawcett, N., Flocculation modeling: a review. *Water Research* **1999,** *33* (7), 1579-1592.